INVESTIGATION OF LOW-VELOCITY DETONATION PHENOMENA IN LIQUID MONOPROPELLANTS AND EXPLOSIVES

Michael Cowperthwaite, et al

Stanford Research Institute

Prepared for:

Air Force Office of Scientific Research

February 1974

SECURITY CLASSIFICATION OF THIS PAGE (When Data Entered)

REPORT DOCUMENTATION PAGE		READ INSTRUCTIONS BEFORE COMPLETING FORM
1. REPORT NUMBER AFOSR - TR - 74 - 0801	2. GOVT ACCESSION NO.	3. RECIPIENT'S CATALOG NUMBER AD-779802
4. TITLE (and Subtitle) INVESTIGATION OF LOW VELOCITY DETONATION PHENOMENA IN LIQUID MONOPROPELLANTS AND EXPLOSIVES (U)		5. TYPE OF REPORT & PERIOD COVERED FINAL 6. PERFORMING ORG. REPORT NUMBER SRI Project PYU 2383
7. AUTHOR(s) MICHAEL COWPERTHWAITE DAVID C ERLICH		8. CONTRACT OR GRANT NUMBER(s) F44620-73-C-0034
9. PERFORMING ORGANIZATION NAME AND ADDRESS STANFORD RESEARCH INSTITUTE 333 RAVENSWOOD AVENUE MENLO PARK, CALIFORNIA 94025		10. PROGRAM ELEMENT, PROJECT, TASK AREA & WORK UNIT NUMBERS 681308 9711-01 61102F
11. CONTROLLING OFFICE NAME AND ADDRESS AIR FORCE OFFICE OF SCIENTIFIC RESEARCH/NA 1400 WILSON BOULEVARD ARLINGTON, VIRGINIA 22209		12. REPORT DATE Feb 1974 13. NUMBER OF PAGES 71
14. MONITORING AGENCY NAME & ADDRESS(if different from Controlling Office)		15. SECURITY CLASS. (of this report) UNCLASSIFIED 15a. DECLASSIFICATION/DOWNGRADING SCHEDULE

16. DISTRIBUTION STATEMENT (of this Report)

Approved for public release; distribution unlimited.

17. DISTRIBUTION STATEMENT (of the abstract entered in Block 20, if different from Report)

18. SUPPLEMENTARY NOTES

19. KEY WORDS (Continue on reverse side if necessary and identify by block number)

LIQUID PROPELLANTS	HUGONIOT CURVES	YTTERBIUM STRESS GAGES
LOW VELOCITY DETONATION	INCOMPLETE REACTION	PRESSURE MEASUREMENTS
HIGH VELOCITY DETONATION	BUBBLE DYNAMICS	
CAVITATION	HEAT AND MASS TRANSFER	
REACTIVE DISCONTINUITIES	SHOCK INITIATION	

20. ABSTRACT (Continue on reverse side if necessary and identify by block number)

Theoretical and experimental studies were conducted to gain a basic understanding of low-velocity detonation (LVD) in confined energetic liquids. The main objective of the theoretical study was to develop satisfactory models for the initiation and propagation of LVD. LVD was modeled as a reactive shock discontinuity propagating in a liquid cavitated by liquid-wall interactions. A study of Hugoniot curves and numerical calculations on burning bubbles were undertaken to determine the amount of reaction required to support the wave. Reactive Hugoniot curves with a positively sloped lower branch and a negatively sloped upper branch

DD FORM 1 JAN 73 1473 EDITION OF 1 NOV 65 IS OBSOLETE

UNCLASSIFIED

SECURITY CLASSIFICATION OF THIS PAGE (When Data Entered)

in the pressure-volume (p-v) plane were constructed to account for LVD and for the transition of LVD into high velocity detonation (HVD) in heterogeneous material. The main objective of the experimental study was to use multiple Lagrangian stress gages to obtain a more accurate and quantitative description of LVD. Ytterbium foil stress gages were used to record stress-time histories in LVD propagating in a nitromethane-tetranitromethane mixture contained in a steel tube. The approximate steady-state stress-time profiles showed that LVD, initiated by pressure in the range 3.6-16 kbar, propagated at 1.87-1.99 mm/μsec with peak pressures in the range 6-10 kbar.

STANFORD RESEARCH INSTITUTE
Menlo Park, California 94025 · U.S.A.

Final Report *February 1974*

INVESTIGATION OF LOW-VELOCITY DETONATION PHENOMENA IN LIQUID MONOPROPELLANTS AND EXPLOSIVES

Authors: M. COWPERTHWAITE and D. C. ERLICH
Contributors: D. C. WOOTEN and JAY LEVINE

Prepared for:

DIRECTOR OF AEROMECHANICS AND ENERGETICS
AIR FORCE OFFICE OF SCIENTIFIC RESEARCH
ARLINGTON, VIRGINIA 22209

CONTRACT F44620-73-C-0034

SRI Project PYU-2383

Approved by:

G. R. ABRAHAMSON, *Director*
Poulter Laboratory

C. J. COOK, *Executive Director*
Physical Sciences Division

CONTENTS

ILLUSTRATIONS

TABLES

INTRODUCTION

The long range objective of the research presented in this report was to develop a basic understanding of low velocity detonation (LVD) and to determine conditions for its initiation and propagation. Such knowledge is required for predicting the LVD behavior of energetic materials used in propulsion systems. It is important to the Air Force because the possibility of initiating LVD with pressures below 10 kbars constitutives a major hazard in the efficient use and manufacture of liquid monopropellants and energetic plasticizer compounds. Events that must be safeguarded against are the malfunction of rocket motors caused by LVD in the fuel container or fuel feed system, and serious accidents caused by LVD during the preparation and transportation of large quantities of such materials.

Shock wave studies during the last decade,[1-6] extending the earlier work discussed by Taylor,[7] have established that most liquid propellants and explosives exhibit two modes of self-sustaining detonation. These modes have distinct velocities of propagation and have been characterized accordingly as high-velocity detonation (HVD) and low-velocity detonation (LVD). HVD propagates at approximately 6 mm/μsec with a pressure in the 100-kilobar region and can be initiated by a shock with a peak pressure of about 60 kilobars. LVD propagates with a slightly higher velocity than ambient sound speed, at approximately 2 mm/μsec with a pressure in the 10-kilobar region, and can be initiated by a shock with a peak pressure of about 4 kilobars. In some cases, however, LVD has been observed to transform into HVD.

Since explosives are required to behave reproducibly and produce pressures in the 100-kilobar region in most practical applications, detonation studies have concentrated on HVD rather than on LVD. Consequently, conditions for initiation and propagation of LVD are not as well established as those for HVD, and our understanding of LVD is not as complete as that of HVD. This situation is further accentuated by the disparity in the theoretical treatments of HVD and LVD. The hydrothermodynamic theory of detonation is satisfactory for modeling the initiation and propagation of HVD and for calculating HVD detonation parameters with the Chapman-Jouguet (C-J) hypothesis when the equation of state of the detonation products is known, but there is no comparable theory for LVD.

BACKGROUND AND APPROACH

Previous research on LVD in Poulter Laboratory at Stanford Research Institute (SRI) was supported by AFOSR under Contract F44620-69-C-0079 and is documented in the final report written for this contract.[8] This research included both theoretical and experimental studies. Computer calculations were performed in the theoretical study to test the cavitation model of LVD,[5] and ytterbium stress gages were used in the experimental study to determine the states attained in LVD waves. A brief discussion of this work is given below as background for the present project.

In the cavitation model, LVD is treated as a reactive shock propagating in a cavitated liquid. The liquid is first cavitated by interactions with the container wall, and reaction is then initiated by bubble collapse in the compressed cavitation field. Computer studies were performed to investigate the cavitation process and to determine the amount of reaction required to support LVD. Two-dimensional computer calculations of a shock propagating in a liquid contained in a cylindrical steel tube showed that precursor wall waves produce regions of tension sufficient to cavitate the liquid before it is compressed by the main shock. Simulation of hot-spot-initiated reaction in the calculations by addition of energy behind the shock led to the conclusion that only part of the chemical energy is required to support the wave. Methods of calculating LVD parameters were formulated with the hydrothermodynamics of the cavitation model, and a complete equation of state for nitromethane was introduced into the TIGER code so that detonation calculations could

be made for incomplete reaction. The calculations showed that only about 20 percent of the liquid is required to react to support LVD and that LVD parameters are insensitive to the initial degree of cavitation. The results of this theoretical study are significant because they place the cavitation model on a firm foundation and justify its use as a basis for further studies to develop a satisfactory treatment of LVD.

Ytterbium gages were used to study LVD in ethyl nitrate and in FEFO. LVD propagation velocities were found to be about 2 mm/μsec in ethyl nitrate and 3 mm/μsec in FEFO; peak pressures were recorded from 4 to 7 kbars.

The present work on LVD was a logical continuation of that discussed above. Theoretical and experimental studies were continued to determine conditions for the onset and termination of reaction in the compressed cavitation field and conditions for the initiation of LVD and its transition into HVD.

Two approaches were taken in the theoretical study. The first approach was a numerical study of bubble dynamics with heat and mass transfer and chemical reaction. The idea was to try to establish conditions for the onset and termination of reaction in a single bubble, and then to try to apply these conditions to the cavitation field to determine the amount of reaction supporting LVD. The computer calculations on a single bubble were performed by J. Levine and D. C. Wooten at Ultrasystems, Inc., and an account of this work is given in the Appendix. The second approach, more empirical than the first, was to study reactive shock discontinuities. Reactive Hugoniot curves were constructed in the pressure-volume (p-v) plane to account for the initiation and propagation of LVD and for its transition into HVD. These approaches will lead to a satisfactory model for LVD when the parameters used in the treatment of reactive shock discontinuities can be evaluated with the results of the computer calculations, and these parameters agree with experimental values.

A new method for placing multiple stress gages in a liquid was devised in the experimental study. This new method of gage emplacement allows the gages to move with the flow and record a more accurate and quantitative description of the states attained in LVD. Experiments using multiple ytterbium stress gages were performed on mixtures of nitromethane and tetranitromethane.

THEORETICAL STUDY OF LVD

LVD Treated as a Reacting Shock Discontinuity

Although a complete treatment of LVD must account for liquid-container wall interactions and the dynamics and thermodynamics of a cavitation field with heat transfer, mass transfer, and chemical reaction, the present work is based on the assumption that a detailed account of these processes is not required to model the initiation and propagation of LVD and its transition into HVD. This approach is motivated by the one-dimensional CJ model for gaseous detonation, which is satisfactory for calculating the average velocity of HVD without treating the complex system of interacting transverse waves necessary for its propagation.

Detonation will be considered as a reactive shock discontinuity and the flow behind it as one dimensional. The time scale for compression and reaction supporting the shock is therefore assumed to be very small compared with the time scale for the subsequent pressure release in the wave. Consequently, HVD is represented as a shock discontinuity with complete reaction, and LVD as a shock discontinuity with incomplete reaction. Let ρ, v, p, and e denote density, specific volume, pressure, and specific internal energy, and let the subscripts H and o denote quantities immediately behind and in front of a shock discontinuity. Then the Rankine-Hugoniot jump conditions expressing the conservation of mass, momentum, and energy across a shock discontinuity propagating into stationary material can be written as

$$p_H v_H = (U - u_H)u_H = v_H U u_H / v_o \qquad (1)$$

$$2(e_H - e_o) = p_H(v_o - v_H) = u_H^2 \qquad (2)$$

where U denotes the shock velocity, u denotes the particle velocity, and the initial pressure p_o has been neglected. Let t and r denote time and distance; then the equations expressing the conservation of mass, momentum, and energy in the flow behind the shock can be written as

$$\frac{d\rho}{dt} + \rho \frac{\partial u}{\partial r} = 0 \tag{3}$$

$$\rho \frac{du}{dt} + \frac{\partial p}{\partial r} = 0 \tag{4}$$

$$\frac{de}{dt} + p \frac{dv}{dt} = 0 \tag{5}$$

where $d/dt = \partial/\partial t + u\partial/\partial r$ and the subscripts on the partial derivatives have been omitted for notational convenience. When the flow is supported by an exothermic reaction described by a reaction coordinate λ, combination of Eq. (5) and the $e = e(p, v, \lambda)$ equation of state leads to the equation

$$\frac{dp}{dt} = c^2 \frac{d\rho}{dt} + \frac{\Gamma}{v} Q \frac{d\lambda}{dt} \tag{6}$$

where $c = (\partial p/\partial \rho)^{\frac{1}{2}}_{s,\lambda}$ denotes the sound speed, s denotes the specific entropy, $\Gamma/v = (\partial p/\partial e)_{v,\lambda}$ is the Grüneisen parameter, and $Q = -(\partial e/\partial \lambda)_{p,v}$ denotes the specific heat of reaction.

To eliminate equation-of-state problems it is assumed that the explosive mixture behaves as a polytropic medium described by an $e(p,v,\lambda)$ equation of state of the form

$$e = e^o_x - \lambda Q + \frac{pv}{K - 1} \tag{7}$$

where K denotes the polytropic index and e^o_x denotes the heat of formation of the explosive. Combination of Eqs. (1) and (2) with Eq. (7) leads to the following equations for a strong reactive shock discontinuity in a polytropic medium,

$$2\,Uu_H = (K+1)u_H^2 + 2(K-1)\,Q\lambda_H \tag{8}$$

$$2\,p_H v_o = (K+1)u_H^2 + 2(K-1)\,Q\lambda_H \tag{9}$$

Let U_D denote the detonation velocity of the CJ discontinuity, and let the subscript CJ denote the Chapman-Jouguet state. Then, substituting $\lambda_{CJ} = 1$ and the CJ condition written as $U_D = (K+1)u_{CJ}$ into Eqs. (8) and (9) yields the following well-known expressions for HVD,[9]

$$U_D^2 = 2(K^2-1)Q \tag{10}$$

$$p_{CJ} = 2(K-1)Q\rho_o \tag{11}$$

The equations for a nonreactive shock discontinuity are obtained by setting $\lambda_H = 0$ in Eqs. (8) and (9). It follows from Eqs. (8) and (9) that the release of chemical energy in a shock discontinuity lowers the values of shock pressure and particle velocity with respect to the values across a nonreactive discontinuity propagating at the same velocity. In other words, the reactive Hugoniot curve lies above the nonreactive Hugoniot in the (p-u) plane.

The differential equation governing the propagation of a shock discontinuity will now be derived. The assumption will also be made that the flow behind the shock is nonreactive. Let $D(\ )_H/Dt = \partial(\ )/\partial t_H + U\partial(\ )/\partial r_H$ denote the directional time derivative along the shock path; then the shock pressure and particle velocity satisfy the following identities

$$\frac{Dp_H}{Dt} = \frac{dp}{dt_H} + (U - u_H)\frac{\partial p}{\partial r_H} \tag{12}$$

and

$$\frac{Du_H}{Dt} = \frac{du}{dt_H} + (U - u_H)\frac{\partial u}{\partial r_H} \tag{13}$$

The combination of Eqs. (12) and (13) with Eqs. (3) and (4), and Eq. (6) subject to the condition $d\lambda/dt_H = 0$, gives the required equation along the shock path as

$$\frac{Dp_H}{Dt} + \rho_o U \frac{Du_H}{Dt} = \rho_H \left((U - u_H)^2 - c_H^2 \right) \frac{\partial u}{\partial r_H} \qquad (14)$$

At this stage the subscript H will be omitted for notational simplicity because we will be dealing only with quantities evaluated at the top of the shock discontinuity.

Our consideration of reactive shock propagation, based on Eq. (14), is an extension of some ideas developed for Ballistic Research Laboratories under Contract No. DA-04-200-AMC-2469(X).[10] The particle velocity gradient at the shock front is always assumed to be positive because this condition is satisfied in most initiation experiments. Reactive discontinuities satisfy the conditions $\lambda \leq 0$ if $U < U_D$, and $\lambda = 1$ if $U \geq U_D$; $D\lambda/dt > 0$ for accelerating shocks, $D\lambda/Dt < 0$ for decelerating shocks, and $D\lambda/dt = 0$ for shock propagating at constant velocity. It is evident on physical grounds that shocks satisfy the condition $Dp/Du > 0$. Consequently, $Dp/Dt > 0$ and $Du/Dt > 0$ for accelerating shocks, $Dp/Dt < 0$ and $Du/Dt < 0$ for decelerating shocks, $Dp/Dt = Du/Dt = 0$ for constant velocity shocks, and reactive Hugoniot curves satisfy the conditions $Dp/D\lambda > 0$ and $Du/D\lambda > 0$ since p and u are functions of λ. Combination of these conditions with Eq. (14) leads to the conclusions that $(U - u)^2 - c^2 > 0$ for accelerating shocks, $(U - u)^2 - c^2 < 0$ for decaying shocks, and that $(U - u)^2 - c^2 = 0$ for constant velocity shocks. With the notation introduced early, for example, the sonic condition expressed by the last equation becomes $U_D = u_{CJ} + c_{CJ}$ for HVD. It is also convenient to denote the propagation of LVD by U_D^*.

Conditions at a sonic point are readily obtained by rewriting the term in brackets on the right-hand side of Eq. (14) as

$$[(U - u)^2 - c^2] = \frac{K + 1}{2K} c^2 \left[\lambda\left(\frac{u_{CJ}}{u}\right)^2 - 1\right] \qquad (15)$$

Equation (15) gives $\lambda(u_{CJ}/u)^2 = 1$ as the condition for a constant velocity reactive shock discontinuity. Since $(U - u)^2 - c^2 = 0$ at a point where a Rayleigh line is tangent to a Hugoniot curve. $\lambda(u_{CJ}/u)^2 = 1$ is also the condition for a Rayleigh line to be tangent to a frozen Hugoniot curve in the (p-u) plane. In other words, $\lambda(u_{CJ}/u)^2 = 1$ defines the locus of sonic states in the (p-u) plane. The locus of sonic states in the (p-v) plane is readily found to be $v = [Kv_o/(K + 1]$.

It follows from Jouguet's Ruie[11] that accelerating shocks satisfy the condition $v_H > [Kv_o/(K + 1]$ and that decelerating shocks satisfy the reverse inequality $v_H < [Kv_o/(K+1]$. Consequently, in the (p-v) plane, accelerating shocks are represented by points that lie to the right of the sonic locus, decelerating shocks are represented by points that lie to the left of the sonic locus, and constant velocity shocks are represented by points lying on the sonic locus.

We are now in a position to consider initiation of detonation when the initial particle velocity $u_i < U_D$, and the initial pressure $p_i < p_{CJ}$. Since weak shocks do not promote detonation, it is assumed that shocks are unreactive until a critical pressure p_i^* is attained. So $\lambda = 0$ for $p_i \leq p_i^*$, and shocks with initial pressures $p_i \leq p_i^*$ lie on the unreactive Hugoniot curve. Let v_i^* denote the volume on the unreactive Hugoniot when $p_i = p_i^*$, and consider the locus of initial states when p_i is increased from p_i^* to p_{CJ}. As p_i approaches p_{CJ}, the initial states must lie to the right of the sonic locus in the (p-v) plane because shocks with $p_i < p_{CJ}$ promote detonation. Moreover

as p_i approaches p_i^*, the initial states must lie to the left of the sonic locus because (p_i^*, v_i^*) lies on the unreacted Hugoniot curve. It follows from these observations that the initial states lie on a curve connecting (p_i^*, v_i^*) to (p_{CJ}, v_{CJ}) and that this curve must intersect the locus of sonic points. Let p^* denote the pressure at this point of intersection and let λ^* denote the corresponding value of the reaction coordinate. Then reactive shocks with initial pressures in the range $p_i^* < p^*$ will decay, and shocks with initial pressures in the range $p^* < p_i < p_{CJ}$ will build up to HVD. Furthermore, it is possible that shocks initiated with $p_i = p^*$ will propagate at constant velocity and that the sonic point will represent LVD. But the stability of such shocks must be considered before it can be concluded that this is indeed the case.

Conditions for the initiation of HVD with $p_i = p_{CJ}$ [10] lead to the conclusion that a sonic point will be stable and represent LVD when initial shock pressures greater than this sonic pressure do not promote further reaction. Shocks with initial pressures higher than the sonic pressure are therefore represented by points on the frozen Hugoniot curve passing through the sonic point. Shocks with pressures lower than the sonic pressure are represented by points on a reactive Hugoniot curve.

Consider the case when there is only one sonic point, say $(p_1^*, [Kv_o/(K+1)]$, and let λ_1^* be the corresponding value of the reaction coordinate. Then the Hugoniot curve exhibits two branches: the lower branch with $0 \le \lambda \le \lambda_1^*$ and $p_i^* \le p_i \le p_1^*$ has a positive slope; the upper frozen branch with $\lambda = \lambda_1^*$ and $p_i \ge p_1^*$ has a negative slope. LVD is represented by the sonic point (p_1^*, λ_1^*). Consequently, shocks with p_i in the range $p_i^* \le p_i < p_1^*$ decay, shocks initiated with $p_i > p_1^*$ decay to LVD, and those initiated with $p_i = p_1^*$ propagate unchanged as LVD with a velocity U_D^*.

Now consider the case when the Hugoniot curve has a similar shape, a positively sloped lower branch and a negatively sloped upper branch, but intersects the sonic locus in two points (p_1^*, λ_1^*) and (p_2^*, λ_2^*) with $p_2^* > p_1^*$ and $\lambda_2^* > \lambda_1^*$. In this case the upper sonic point represents LVD. Shocks with p_i in the range $p_i^* \leq p_i < p_1^*$ decay, shocks with $p_i > p_2^*$ decay to LVD, shocks with p_i in the range $p_1^* \leq p_i < p_2^*$ build up to LVD, and shocks with $p_i = p_2^*$ propagate at constant velocity as LVD.

As indicated by the computer studies of bubbles, such a situation would occur in the cavitation model when the reaction initiated by bubble collapse is terminated by bubble expansion and does not go to completion. Relationships for Hugoniots exhibiting these two branches were formulated because a Hugoniot of this type was observed by Evans et al.[12] in a shock initiation study of low density pressings of ammonium perchlorate sponsored by AFOSR under Contract AF49(638)-1124.

The transition of LVD into HVD is accounted for by assuming that there is another critical pressure p_i' for the onset of bulk reaction. In this case reaction initiated by bubble collapse at the pressure p_i' is not terminated at later times. Bulk reaction, therefore occurs at the pressure p_i' on the frozen Hugoniot curve passing through the sonic point representing LVD. The locus of shocked states with p_i in the range $p_i' \leq p_i \leq p_{CJ}$ forms a curve that again intersects the sonic locus and has a positive slope in the neighborhood of p_i' and a negative slope in the neighborhood of p_{CJ}. While shocks with initial pressure higher than the pressure at this sonic point build up to HVD, shocks with lower pressures decay to LVD. In most cases, however, HVD propagating in the cavitated liquid will eventually becomes HVD propagating in virgin liquid. HVD in cavitated liquid will usually produce HVD in virgin liquid because it outruns the cavitation field and produces a shock in virgin liquid that is strong enough to produce HVD.

Construction of Hugoniot Curves for the Initiation and Propagation of LVD

Relationships for Hugoniot curves with a positively sloped lower branch and a negatively sloped upper branch were formulated to account for the initiation and propagation of LVD. The condition for a Hugoniot to have a positive slope will be derived first, however, because Hugoniot curves are usually found to have a negative slope. The equation for the slope of a Hugoniot is readily obtained as

$$\frac{dp}{dv}\left[\left(\frac{\partial e}{\partial p}\right)_{v,\lambda} - \tfrac{1}{2}(v_o - v) - Q\frac{d\lambda}{dp}\right] = -\left[\tfrac{1}{2}p + \left(\frac{\partial e}{\partial v}\right)_{p,\lambda}\right] \qquad (16)$$

by eliminating de from the differential forms obtained by differentiating Eq. (2) and the $e = e(p,v,\lambda)$ equation of state. Since we are considering a case in which $(\partial e/\partial p)_{v,\lambda} > 0$, $(\partial e/\partial v)_{p,\lambda} > 0$, and $2(\partial e/\partial p)_{v,\lambda} > (v_o - v)$, it follows from Eq. (16) that the slope of a reactive Hugoniot is positive only when the reaction term $Q\, d\lambda/dp$ is large enough to make the term in brackets on the right-hand side of Eq. (16) negative.

The equation for a reactive Hugoniot curve for our polytropic material is readily obtained as

$$p\left[v\,\frac{(K+1)}{(K-1)} - v_o\right] = 2Q\lambda = \frac{p_{CJ}v_o\lambda}{(K-1)} \qquad (17)$$

by eliminating e from Eqs. (2) and (7), and making use of Eq. (11). Setting $\lambda = 0$ in Eq. (17) gives $v = (K-1)/(K+1)v_o$ for a strong nonreactive shock, and setting $\lambda = 1$ in Eq. (17) gives the equation for the fully reacted Hugoniot curve. The condition $p_{CJ}\lambda^*/p^* = 1$ for a sonic point on a Hugoniot curve is readily obtained by setting $v = [Kv_o/(K+1)]$ in Eq. (17). It is convenient for computational purposes to set $K = 3$, and rewrite Eq. (17) as

$$\frac{v}{v_o} - \tfrac{1}{2} = \frac{\lambda}{4}\frac{p_{CJ}}{p} \tag{18}$$

Equation (18) gives the equation for the slope of this Hugoniot as

$$\frac{dp}{dv}\left(v - \frac{v_o}{2} - Q\frac{d\lambda}{dp}\right) = -p \tag{19}$$

and it follows from Eq. (19) that the Hugoniot has a positive or a negative slope depending on whether $v < (v_o/2 + Qd\lambda/dp)$ or $v > (v_o/2 + Qd\lambda/dp)$.

It follows from Eq. (18) that the specification of either a $v = v(\lambda)$ relationship or a $p = p(\lambda)$ relationship defines a reactive Hugoniot curve. In the present work, however, $\lambda = \lambda(p)$ relationships were formulated to generate Hugoniots with the properties required to account for the initiation and propagation of LVD and for its transition into HVD. For notational simplicity, v_o and p_{CJ} were used to denote the initial specific volume of the cavitated liquid and its CJ pressure, and v_o' and p_{CJ}' were used to denote these quantities for virgin liquid. Values for the initial volumes of virgin and cavitated liquid, the HVD propagation velocity, and the critical pressure for the onset of reaction were chosen, respectively, as $v_o' = 1$ cc/gm, $v_o = 1.25$ cc/gm, $U_D = 6$ mm/μsec, and $p_i^* = 2$ kbar. The CJ condition gives $c_{CJ} = 4.5$ mm/μsec and $u_{CJ} = 1.5$ mm/μsec, and Eq. (11) gives $p_{CJ}' = 90$ kbar and $p_{CJ} = 72$ kbar for the CJ pressure attained in virgin and cavitated liquid, respectively.

The unreacted and fully reacted Hugoniot curves for cavitated liquid obtained by setting $\lambda = 0$ and $\lambda = 1$ in Eq. (18) are shown in Figure 1. The unreacted curve $v/v_o = 0.5$ is shown as NR, and the fully reacted curve as ECD. The point N represents the criticality condition for onset of reaction in the cavitation field, and the point C represents the CJ point for HVD. The sonic locus $v/v_o = 0.75$ is also shown in Figure 1 as SC.

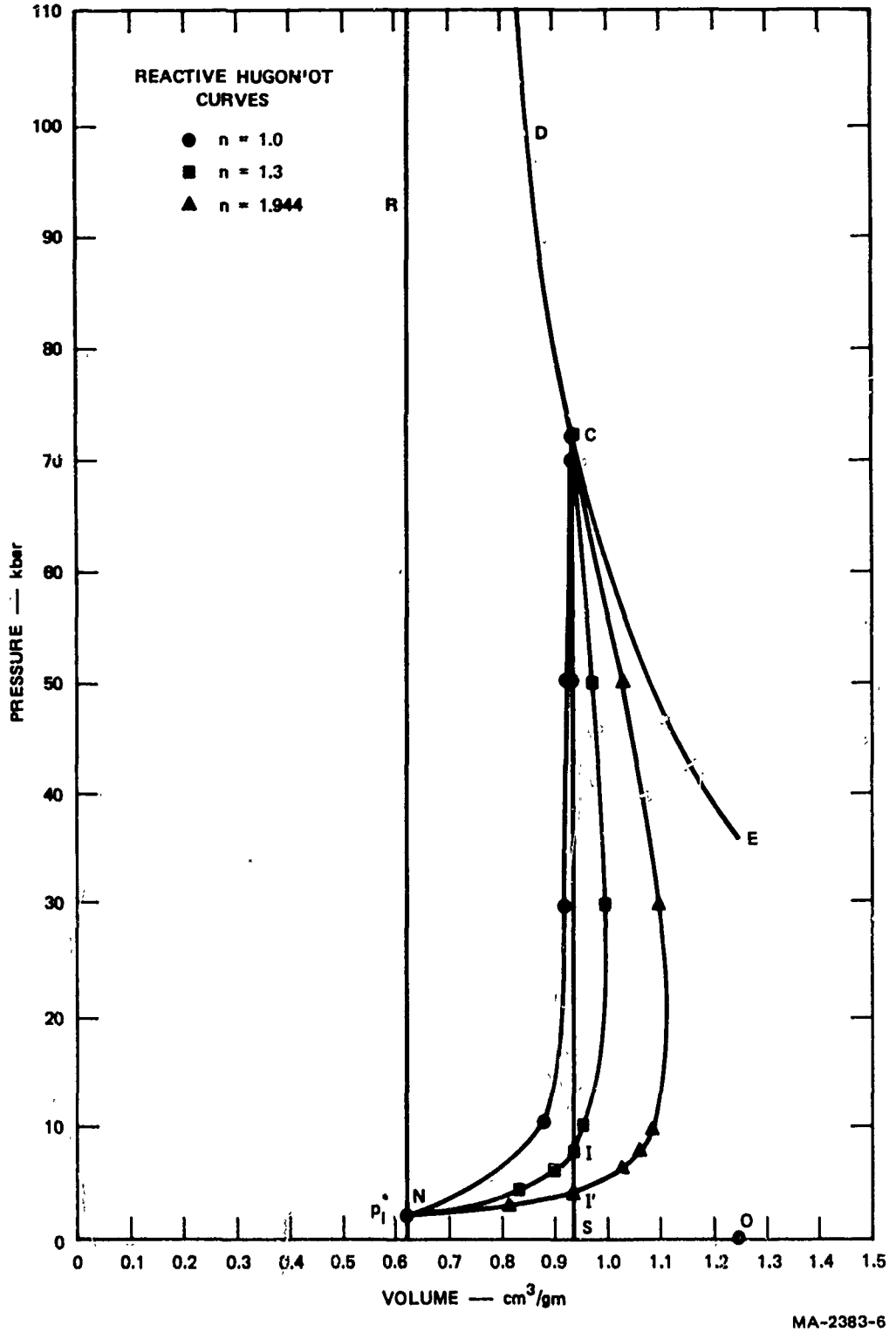

FIGURE 1 REACTIVE HUGONIOT CURVES FOR CAVITATED LIQUID

A $\lambda = \lambda(p)$ relationship for constructing reactive Hugoniot curves connecting N and C was first formulated. Since $\lambda = 0$ when $p = p_i^*$, and $\lambda = 1$ when $p = p_{CJ}$ on these curves, the $\lambda = \lambda(p)$ relationship was chosen simply as

$$\lambda = 1 - \left[\frac{1 - p/p_{CJ}}{1 - p_i^*/p_{CJ}}\right]^n \qquad (20)$$

to satisfy these conditions. Values of the parameter n are restricted, however, by the conditions that the slope of a reactive Hugoniot curve must satisfy at C and N. Values of n must be chosen so that the reactive Hugoniot curve satisfies the CJ condition $(dp/dv)_{CJ} = -K(p/v)_{CJ}$ at C. They must also be chosen so that $Du/D\lambda > 0$ at N to ensure that shocks satisfy the condition $Dp/Du \geq 0$. Equation (19) shows that a reactive Hugoniot satisfies the CJ condition if $d\lambda/dp = 0$ when $\lambda = 1$, and differentiating, Eq. (20) shows that the latter condition is satisfied when $n > 1$. Differentiation of the equation $2u^2/v_o = (p - \lambda p_{CJ}/2)$ obtained by combining Eqs. (2) and (18) gives $n < 2(1 - p_i^*/p_{CJ}) = 1.944$ as the condition that n must satisfy to ensure that $Du/D\lambda > 0$ at N. Values of $n \geq 2(1 - p_i^*/p_{CJ})$ give $Dp/Du < 0$ at N, and the value $n = 2(1 - p_i^*/p_{CJ})$ gives a Hugoniot in the (p-u) plane with an infinite slope at $p = p_i^*$. The additional conditions on the derivatives at C and N therefore restrict the values of n to the range $1 < n < 1.944$.

Equations (18) and (20) were used to calculate reactive (p-v) Hugoniots for different values of n; the results are given in Table I. The limiting values $n = 1$ and $n = 1.944$ were used to determine the domain of the (p-v) plane covered by the family of reactive Hugoniots defined by Eq. (20). The Hugoniot curves calculated with $n = 1$, 1.3, and 1.944 are shown in Figure 1. Examination of Figure 1 shows that while the curve with $n = 1$ does not have a sonic point below C, the

Table I

REACTIVE HUGONIOT CURVES FOR CAVITATED LIQUID

	n = 1		n = 1.3		n = 1.5		n = 1.944	
p (kbar)	v (cc/gm)	λ	v (cc/gm)	λ	v (cc/gm)	λ	v (cc/gm)	λ
3	0.732	0.014	0.764	0.019	0.786	0.021	0.832	0.028
4	0.785	0.029	0.833	0.037	0.864	0.042	0.932	0.055
6	0.839	0.057	0.901	0.074	0.942	0.084	1.030	0.108
8	0.866	0.086	0.934	0.110	0.979	0.126	1.075	0.160
10	0.882	0.114	0.954	0.146	0.100	0.167	1.098	0.210
30	0.925	0.400	0.989	0.485	1.026	0.535	1.097	0.630
50	0.9336	0.686	0.975	0.778	0.996	0.824	1.028	0.895
70	0.937	0.971	0.943	0.990	0.945	0.995	0.946	0.999

curve with $n = 1.3$ has a sonic point I at a pressure of ≈ 8 kbar, and the curve with $n = 1.944$ has a sonic point I′ at a pressure of ≈ 4.5 kbar. Since LVD pressures lie in the 6 to 9 kbar range, values of n in the range $1 < n < 1.944$ can be used to model LVD. The sonic point I ($p = 8.3$ kbar, $\lambda = 0.115$) on the reactive Hugoniot with $n = 1.3$ was chosen to represent LVD because this state is attained in a shock propagating at a velocity of 2.1 mm/μsec and the typical propagation velocity of LVD is $U_D^* \approx 2$ mm/μsec.

We are now in a position to construct Hugoniot curves with either one sonic point (p_1^*, λ_1^*) or with two sonic points (p_1^*, λ_1^*) and (p_2^*, λ_2^*), which were proposed earlier in this report to account for LVD. The case when a Hugoniot has one sonic point will be considered first.

In the first case, $p_1^* = 8.3$ kbar and $\lambda_1^* = 0.115$ since I was chosen to represent LVD. The lower, reactive branch of the Hugoniot with a positive slope is determined by Eqs. (18) and (20), with $n = 1.3$ and with p and λ subject to the conditions $(p_1^* = 2 \text{ kbar}) \leq p \leq (p_1^* = 8.3 \text{ kbar})$ and $0 \leq \lambda \leq 0.115$. The upper, nonreactive branch of the Hugoniot with a negative slope is determined by Eq. (18) with $p \geq p_i^* = 8.3$ kbar and $\lambda = \lambda_1^* = 0.115$. The Hugoniot curve calculated according to this prescription is shown as NIF in Figure 2 where the Rayleigh lines representing LVD and HVD are shown respectively as OI and OC

In the second case, $p_2^* = 8.3$ kbar and $\lambda_2^* = 0.115$. A reactive Hugoniot that connects N and I and has two points of intersection with the sonic locus SC will now be constructed. It is clear from the reactive Hugoniot curves shown in Figure 1 that a $\lambda = \lambda(p)$ relationship producing Hugoniot curves with the desired properties can be obtained by scaling Eq. (20). A $\lambda = \lambda(p)$ relationship for reactive Hugoniot curves with two sonic points was therefore formulated by setting

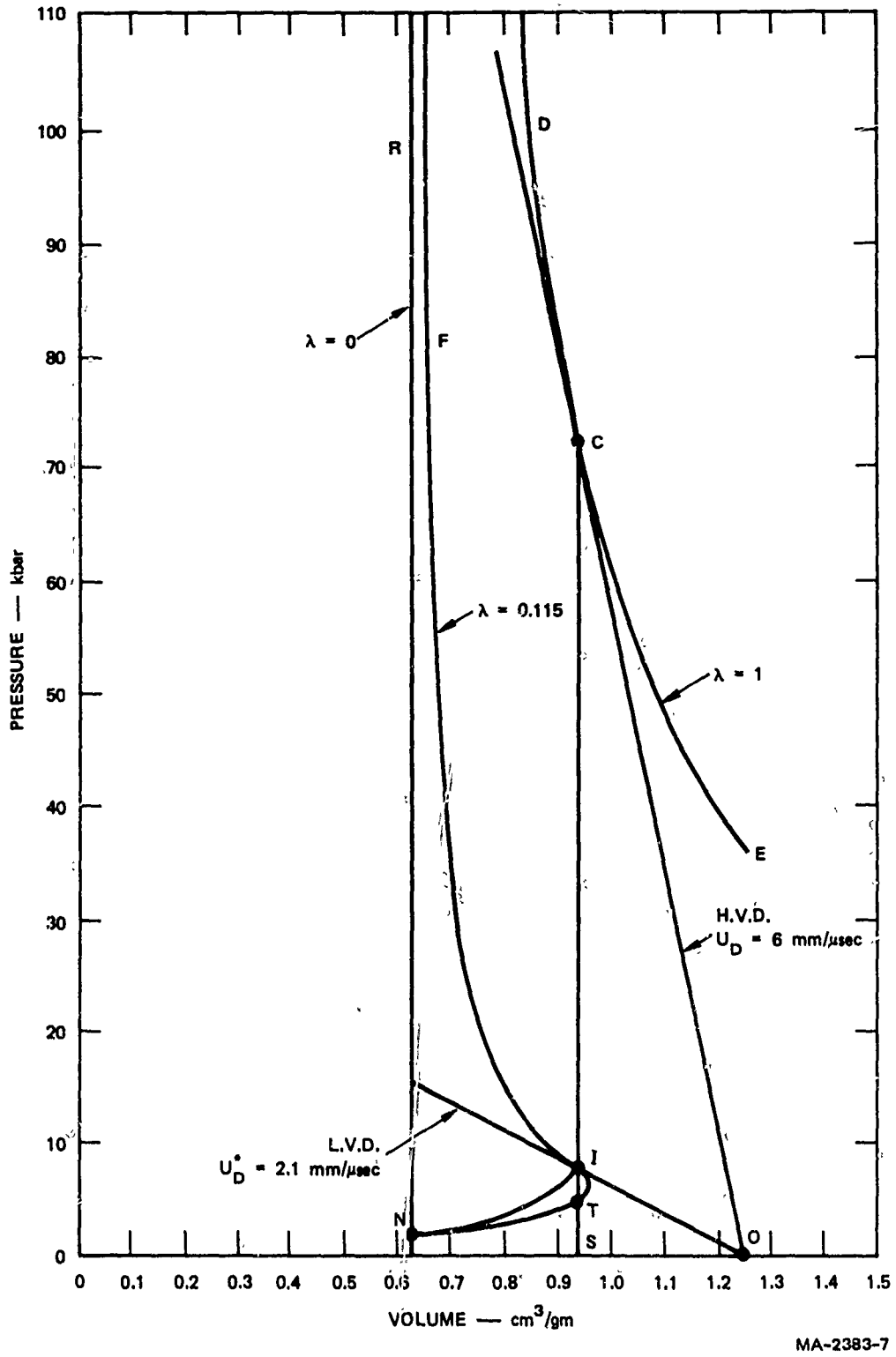

FIGURE 2 HUGONIOT CURVES TO ACCOUNT FOR THE INITIATION AND PROPAGATION OF LVD

$$\lambda = \lambda_2^* \left[1 - \left(\frac{1 - p/p_2^*}{1 - p_i^*/p_2^*}\right)^n\right] \qquad (21)$$

Application of an argument similar to the one used previously for curves with one sonic point, however, shows that n in this case is restricted to the range $1 < n < 2(1 - p_i^*/p_2^*) = 1.52$. The lower reactive branch of the Hugoniot curve with two sonic points is determined for these values of n by Eq. (18) and (21), with p and λ subject to the conditions $(p_i^* = 2 \text{ kbar}) \leq p \leq (p_2^* = 8.3 \text{ kbar})$ and $0 \leq \lambda \leq 0.115$. The upper frozen branch of the Hugoniot is determined, as before, by Eq. (18) with $p \geq p_i = 8.3$ kbar and $\lambda = \lambda_2^* = 0.115$. Reactive Hugoniot curves connecting N and I were calculated, and the results of the calculations performed for $n = 1.3$ and 1.5 are shown in Table II. The reactive curve calculated with $n = 1.5$ is shown in Figure 2 as NTI, and the corresponding Hugoniot constructed to account for the initiation and propagation of LVD is shown as NTIF. The lower sonic point is located at the point T with a pressure $p_1^* \sim 4.5$ kbar.

Since $p_1^* \sim 4.5$ kbar and $p_2^* = 8.3$ kbar, LVD modelled with NTIF will exhibit the following properties. Shocks with initial pressures $p_i < \sim 4.5$ kbar will decay, shocks with initial pressures in the range $8.3 > p_i > \sim 4.5$ kbar will build up to LVD, and shocks with $p_i > 8.3$ but less than the critical pressure for onset of bulk reaction will decay to LVD.

Although the transition of LVD into HVD will not be considered further in this report, it is clear that $\lambda = \lambda(p)$ relationships, producing curves similar to the reactive Hugoniots shown in Figure 1, can easily be formulated to account for this type of behavior.

Table II

REACTIVE HUGONIOT CURVES FOR LVD

p (kbar)	n = 1.3		n = 1.5	
	v (cc/gm)	λ	v (cc/gm)	λ
2	0.625	0.0	0.625	0.0
3	0.799	0.023	0.823	0.026
4	0.879	0.045	0.907	0.050
5	0.920	0.066	0.947	0.072
6	0.940	0.084	0.963	0.090
7	0.948	0.100	0.961	0.105
8	0.943	0.113	0.946	0.114
8.3	0.938	0.115	0.938	0.115

EXPERIMENTAL STUDY OF LVD

The objective of the experimental phase of the program was to obtain a more accurate and quantitative description of LVD. Shock wave experiments using multiple ytterbium stress gages were designed and performed to achieve this objective. A new method of gage emplacement was developed to allow the gages to move with the flow so that the experiments would provide stress histories at different Lagrangian positions in a liquid undergoing LVD.

The new method of gage emplacement is a definite improvement over the previous method,[12] which was developed for AFOSR under Contract F44620-69-C-0079 and used to study LVD in ethyl nitrate and FEFO. In these previous experiments, the ytterbium gages were placed in the direction of the flow. The gage records were suitable for measuring shock arrival time and for determining propagation velocity, but later interpretation was difficult because it was not known whether the gages recorded predominantly Lagrangian or Eulerian stress histories. Furthermore, placement of gages in the direction of the flow caused their response time to be large (> 250 nsec). Consequently in the current program, the gages were placed perpendicular to the direction of the flow so that they would move with the liquid and record Lagrangian stress histories with a smaller response time.

Six experiments were performed in the SRI explosives vault facility using a mixture of tetranitromethane (4 parts by weight) and nitromethane (5 parts by weight) in a steel tube into which several ytterbium stress gages had been emplaced to record Lagrangian stress histories.

A schematic diagram of the experiments is shown in Figure 3. A cylindrical seamless cold-rolled steel tube was used to contain the liquid. The tube was 14-in. long, had an inside diameter of 3/4 in., a wall thickness of 1/8 in., and was filled with liquid to within an inch of its top. The explosive donor system consisted of a bridgewire detonator, a tetryl booster pellet, a 2-in.-diameter by 2-in.-thick tetryl explosive pad, and a 3-in.-diameter Homalite* attenuator. The detonation in the tetryl pad was initiated by the exploding bridgewire and the tetryl pellet, and the thickness of the attenuator was chosen to produce the desired shock pressure entering the liquid.

Two to four stress gages were positioned from 2 to 8 inches above the bottom of the tube. A typical four-terminal ytterbium foil grid gage element is shown in Figure 3. This element was attached to a thin layer of Homalite-impregnated fiberglass and covered with a thin layer of Homalite to form a total gage package with a thickness of ≈ 6 mils. The gage package was cut to fit snugly into the steel tube, with two segments removed as shown in Figure 3 so that the tube could be filled with liquid, and was supported by a thin layer of glue. A 1/8-in. hole was drilled through the tube approximately an inch above each gage package location, and the leads from each gage were brought out through this hole. This method of emplacement ensured that the gage would survive long enough to record the LVD pulse. Had the gage leads been brought straight out at the same level as the gage package, they would have sheared off as the liquid flowed along the inside wall of the tube.

An additional ytterbium stress gage was placed at or near the Homalite attenuator-liquid interface to record the stress pulse entering the liquid.

---

*Trade name, Homalite Corporation.

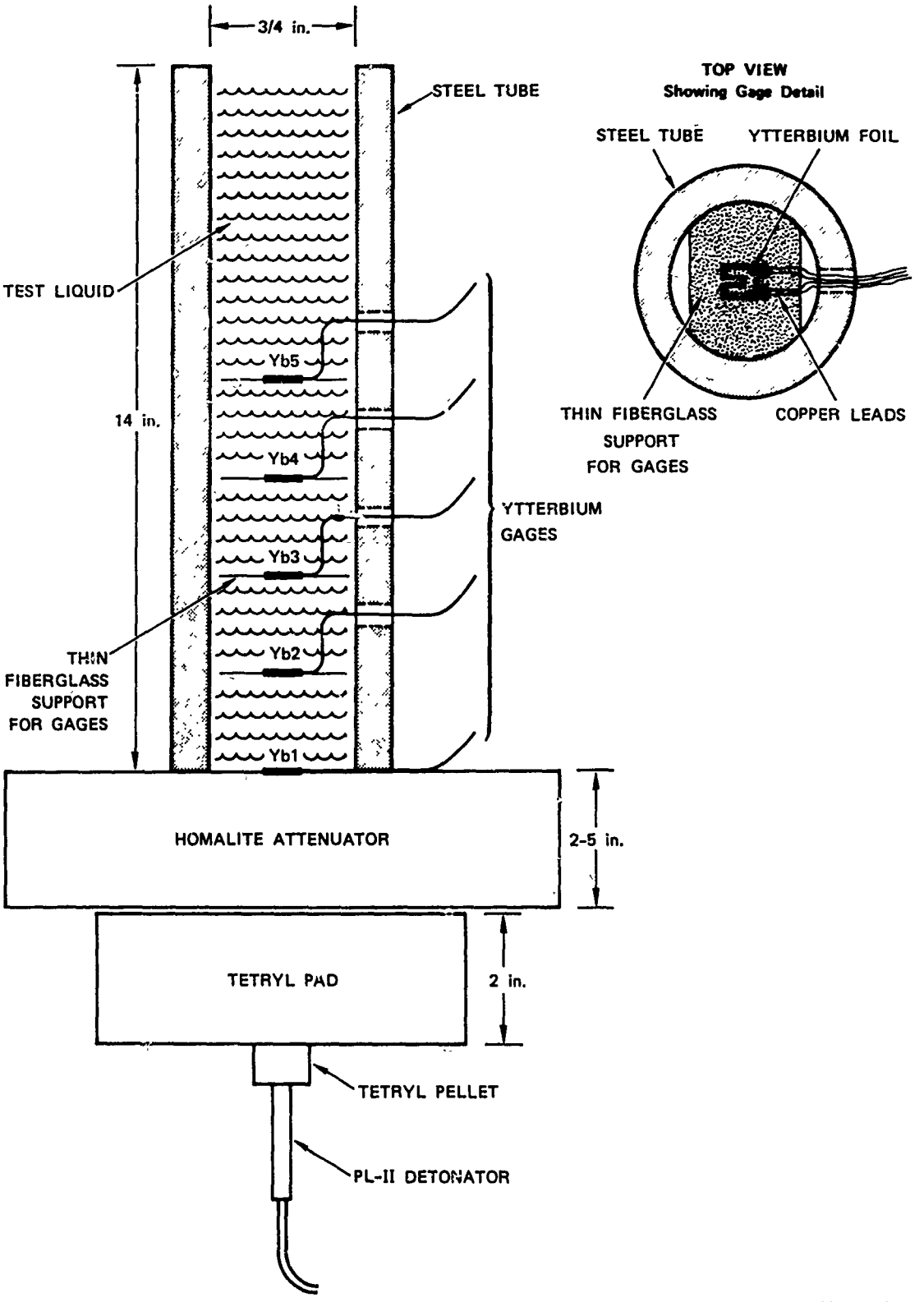

FIGURE 3 SCHEMATIC DIAGRAM OF LVD EXPERIMENTS

The gage records were calibrated using the formula given by Ginsberg[13] for calibration of ytterbium foil for the region from 0 to 10 kbar.

Of the six experiments attempted, all but one yielded satisfactory data. The one that failed was shot 2, using a 2-in.-thick Homalite attenuator. Post-shot recovery of the tube fragments indicated that shot 2 experienced a high-velocity detonation (HVD). Two other shots in this series used the same attenuator thickness and therefore had nearly the same stress pulse magnitude enter the liquid; these two shots exhibited LVD.

The relevant parameters for the five successful shots are shown in Table III, along with the peak stresses recorded by the various gages and the velocity of the compressional part of the LVD wave. The five experiments span a range of peak stress incident upon the liquid from 3.6 to 16 kbar.

The oscillographs from the stress gages in shot 3 are shown in Figure 4. Three gages recorded in the liquid at 2, 4, and 6 inches above the liquid-Homalite interface, and a fourth gage recorded just below the interface. The fourth gage, Figure 4(d), shows a peak stress equal to the stress in the Homalite and then a decrease to the stress entering the liquid (the liquid has a lower shock impedance than the Homalite, hence the difference).

All the in-liquid stress histories recorded for all five shots show features similar to those shown in Figure 4 (a), (b), and (c). These include a rapid rise or shock to a peak pressure of from 6.0 to 9.1 kbar, a shock velocity between successive gages of from 1.87 to 1.99 mm/μsec, and a decay to nearly zero stress of several microseconds duration. There is no noticeable variation (to within the statistics of these experiments)

Table III

EXPERIMENTAL PARAMETERS AND RESULTS FOR LVD SHOTS

Shot No.	1	3	4	5	6
Attenuator thickness (in.)	2	3-1/32	3-1/32	2-1/32	5-1/32
Peak stress entering liquid[a] (kbar)	16	6.1	8.4	b	3.6
First in-liquid gage:					
Height in tube (in.)	2	2	2	2	2
Recorded peak stress (kbar)	7.25	7.4	8.15	7.2	7.25
Second in-liquid gage:					
Height in tube (in.)	5	4	4	4	4
Recorded peak stress (kbar)	8.15	8.6	7.5	6.0	10.3[c]
Measured velocity[d] (mm/μsec)	1.96	1.95	1.96	1.99	1.96
Third in-liquid gage:					
Height in tube (in.)	--	6	6	--	6
Recorded peak stress (kbar)	--	9.1	8.25	--	8.6
Measured velocity (mm/μsec)	--	1.93	1.87	--	1.92
Fourth in-liquid gage:					
Height in tube (in.)	--	8	8	--	8
Recorded peak stress (kbar)	--	b	7.8	--	8.15
Measured velocity (mm/μsec)	--	1.92	1.91	--	1.89
Average peak stress for in-liquid gages (kbar)	7.7	7.7	8.0	6.6	8.0
Average measured velocity (mm/μsec)	1.96	1.93	1.91	1.99	1.92

a. As measured by gage at Homalite-liquid interface.
b. Data of insufficient quality to analyze.
c. Questionable data, not used in averages.
d. Measured velocity is that of the midpoint of the compressive shock between this and the previous gage location.

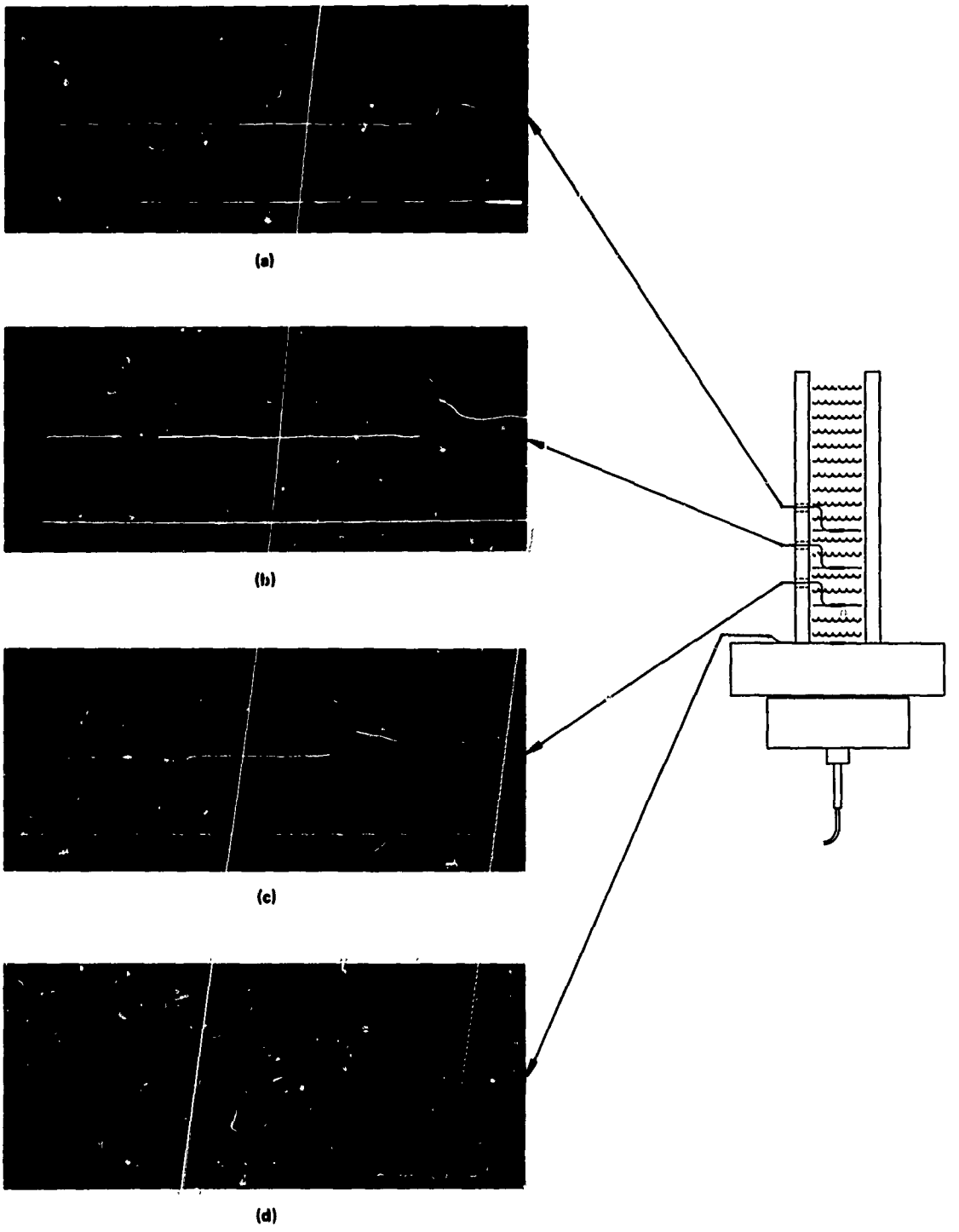

FIGURE 4 OSCILLOGRAPHS FROM LVD SHOT 3

in peak pressure or shock velocity as a function of incident stress into the liquid. In other words the LVD wave attains the same approximate peak pressure and shock velocity regardless of the magnitude of the initiating shock. Furthermore this approximately steady wave is nearly attained within the first two inches of the liquid, as shown by the closeness of the average peak stress measured at the 2-in. location (7.4 kbar) compared with the overall average peak stress (7.6 kbar) and the similarity of the average shock velocity measured between the 2-in. and the next gage location (1.96 mm/μsec) to the overall average (1.93 mm/μsec).

Figure 5 is a plot of the arrival times of the midpoint of the LVD shock, in microseconds from the time the shock enters the liquid, as a function of the Lagrangian position or initial location of the gage plane in the liquid. The lines for all five shots are very straight and nearly parallel, indicating constant velocity. The only difference is in their vertical position on the graph. For example, the LVD wave for shot 6 arrives 3 μsec later than that for shot 1. Since the stress entering the liquid in shot 1 is 16 kbar, while that in shot 6 is only 3.6 kbar, the difference in arrival times is caused by a combination of the following two factors: (1) The shock velocity of the unreacted liquid before LVD initiation is higher at higher stresses because of the concave upward nature of the liquid Hugoniot. (2) The LVD might take longer to initiate at lower stresses. Further experimentation is necessary, however, to determine which of these factors is more important.

The in-liquid stress gage records for shots 3 and 6 were digitized and plotted together in Figures 6(a) and 6(b), respectively. The horizontal or time axis was shifted so that the first motion or the foot of the compressional shock for all three gages coincided at zero time.

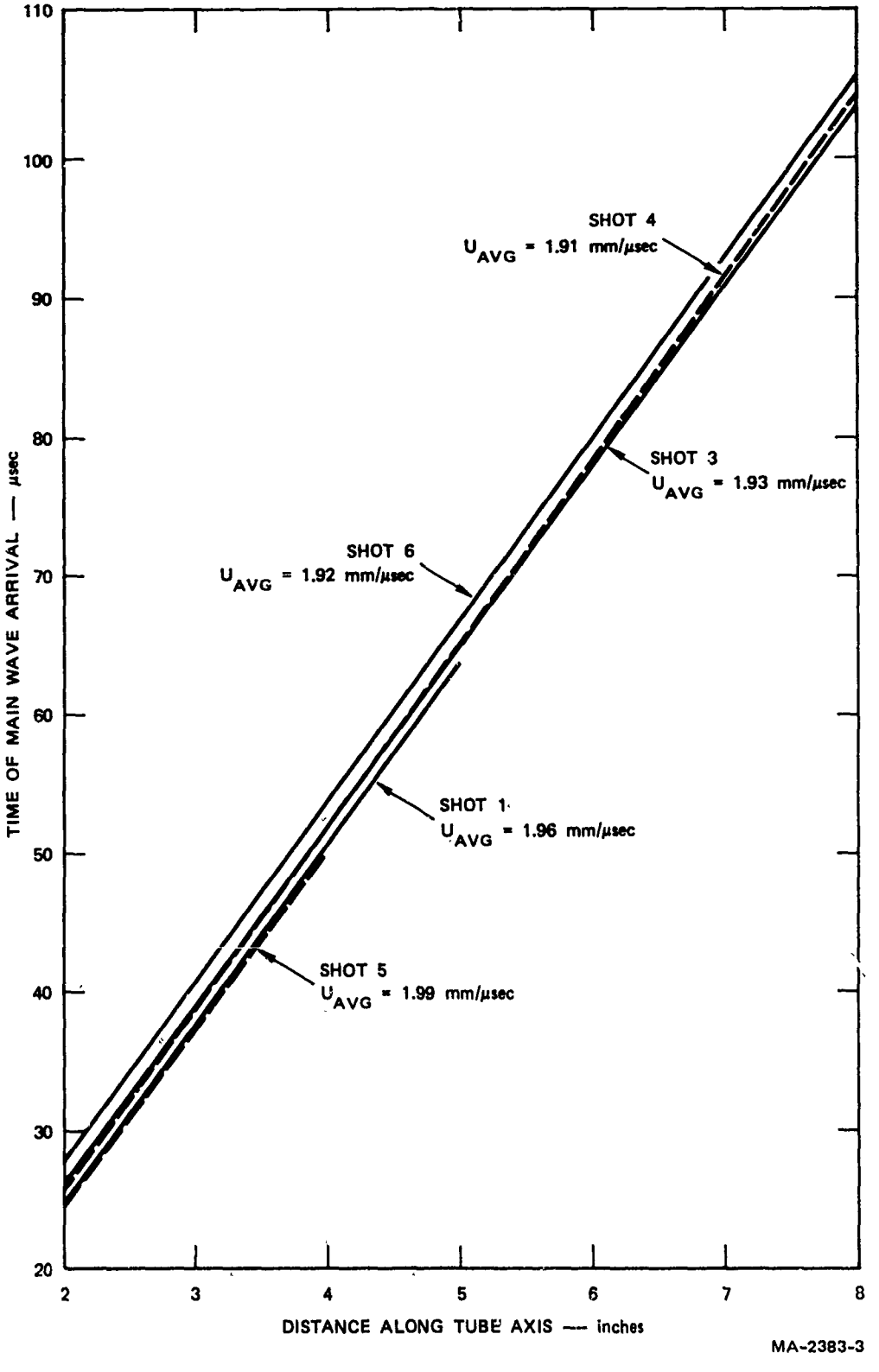

FIGURE 5 DISTANCE-TIME PLOT OF MIDPOINT OF LVD COMPRESSIONAL WAVE FOR ALL 5 EXPERIMENTS

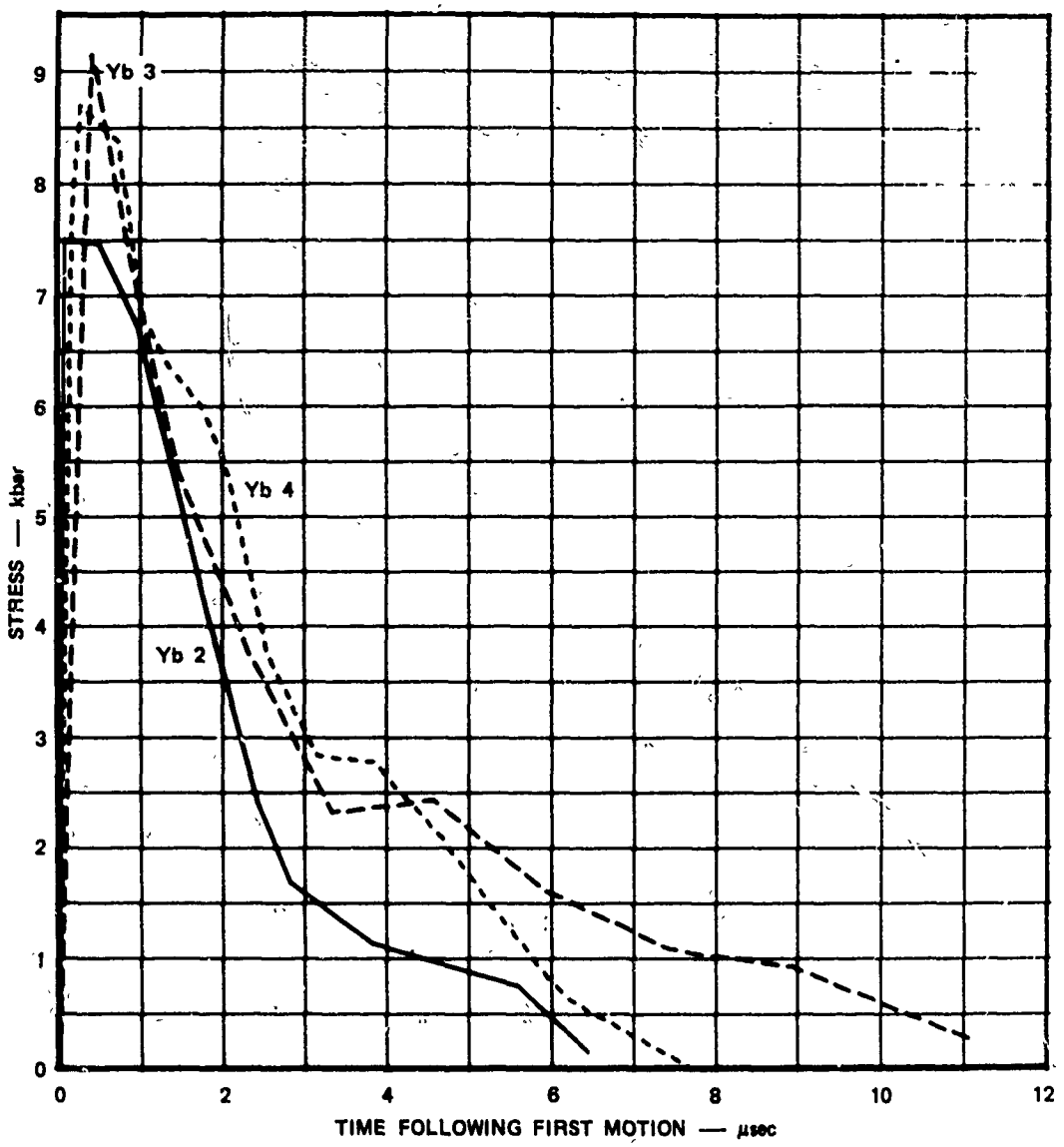

(a) FROM SHOT 3

MA-2383-4

FIGURE 6 COMPOSITE STRESS HISTORIES OF IN-LIQUID YTTERBIUM GAGES

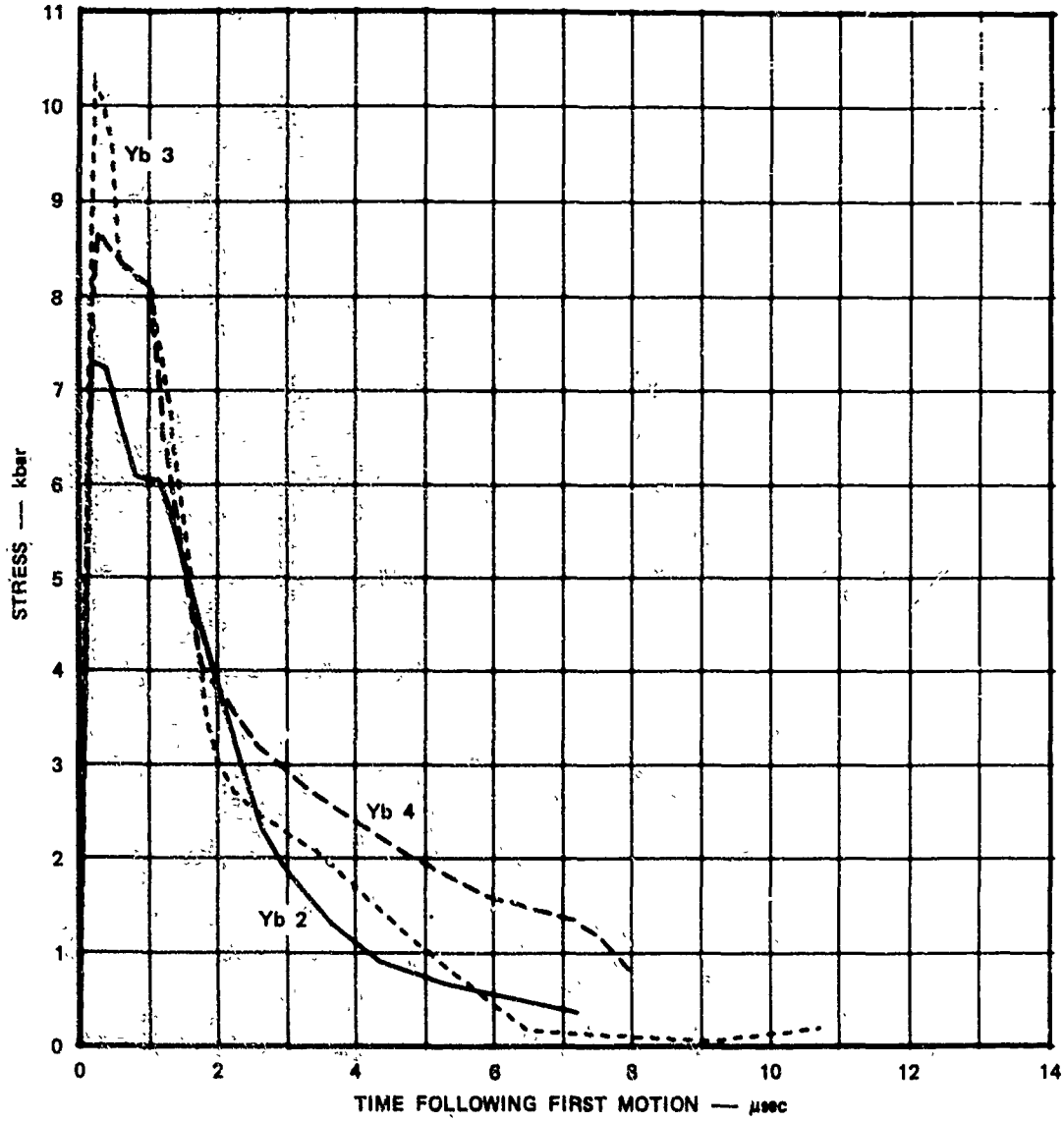

(b) FROM SHOT 6

MA-2383-5

FIGURE 6 COMPOSITE STRESS HISTORIES OF IN-LIQUID YTTERBIUM GAGES (concluded)

If LVD were precisely steady state throughout the region of measurement, each point in the wave would travel at the same velocity, and as a consequence the recorded stress histories would be exactly congruent.

The actual results are fairly congruent in each case except in two regions--near the peak and at the final third of unloading. The peak stress of the first gage is significantly lower than that of the other two for both shots 3 and 6, indicating that perhaps the LVD has not yet reached its maximum or steady-state stress level in the first two inches of liquid. The unloading is slower for gages farther up the tube, which indicates that the release wave velocity is less than that of the compressional wave. The lower velocity of the release wave is quite likely because the liquid is in a heated state following detonation; however, the difference is very small. In shot 3, the release velocity at 4 kbar is only 1% lower than the shock velocity, and from there the difference increases to a maximum of 8% at 1 kbar. For shot 6, the differences are even smaller.

In conclusion, we have successfully obtained Lagrangian stress histories in a liquid undergoing LVD. The records indicate that the compressional part of the LVD wave propagates at very nearly constant peak stress and velocity, while the release portion of the LVD wave, although initially nearly steady state, begins to diverge (i.e., propagate at slightly lower velocities) as the stress decays to zero. This technique can now be used with a high degree of certainty of success to study in detail the initiation and propagation of LVD.

CONCLUSIONS

Considerable progress has been made in a basic understanding of LVD and in determining conditions for its initiation and propagation.

The treatment of reactive shocks formulated in the theoretical study provides for the first time a simple model to account for the initiation and propagation of LVD. Shocked states are described by Hugoniot curves that exhibit two sonic points in the region of 2 to 10 kbar. The sonic point with the higher pressure p_2^* represents LVD, and the sonic point with the lower pressure p_1^* defines the initial pressure needed for shocks with a positive particle velocity gradient to build up to LVD. If p_i denotes the initial shock pressure, then shocks decay when $p_i < p_1^*$, build up to LVD when $p_1^* \leq p_i < p_2^*$, and decay to LVD when $p_i > p_2^*$.

The development of multiple ytterbium gages to determine Lagrangian stress histories in shocked liquids provides a means of obtaining a more accurate and quantitative description of the states attained during the initiation and propagation of LVD. The stress histories recorded by the ytterbium gages in a tetranitromethane-nitromethane mixture lead to the following conclusions about LVD in this liquid. The compressional part of the LVD wave propagates at constant velocity with a constant peak pressure; the flow in the release part of the wave is steady state as the pressure falls to one-half or one-third of the peak pressure and then becomes unsteady.

The results of the experiments show that LVD in the tetranitromethane-nitromethane mixture is initiated by shocks with initial pressures in the

3.6 to 16 kbar range, and the reactive Hugoniot curves constructed in the the theoretical study lead to the conclusion that shocks will build up to LVD when their initial pressures are greater than $\sim$ 4.5 kbar, and will decay to LVD when their initial pressures are greater than $\sim$ 8.5 kbar.

Additional work is required, however, to develop a more fundamental treatment of LVD because the work on reactive shock discontinuities is semiempirical, and because the computer calculations on burning bubbles did not provide a condition for calculating the degree of incomplete reaction in the compressed cavitation field. To be more specific, LVD pressure is a parameter that must be known, and the critical pressure for onset of reaction in the cavitation field and the relationship for the reactive Hugoniot curve were chosen rather than calculated from first principles. The calculations on burning bubbles did not provide conditions for evaluating these quantities because the calculations were performed for a contracting bubble in an incompressible liquid, and the reaction is probably extinguished during bubble expansion when compressibility factors cannot be ignored. It is therefore necessary to formulate a satisfactory model for determining the amount of reaction in the compressed cavitation field as a function of pressure so that all these quantities can be calculated. A study of reactive bubbles in a compressible liquid undergoing contraction and expansion should be continued to develop such a model. A study of reactive shock propagation including divergence and reaction behind the shock should also be undertaken to test the assumption that LVD can be treated as a one-dimensional wave.

ACKNOWLEDGMENT

The authors thank R. W. Woolfolk, C. M. Tarver, and M. Ginsberg for helpful discussions. We are also greatly indebted to R. W. Woolfolk for testing the detonability of the nitromethane-tetranitromethane mixture and for preparing the samples for the shock wave experiments, and to B. Y. Lew for digitizing the gage records.

REFERENCES

1. L. G. Bolkhovitinov, Dokl. Akad. Nauk SSSR 130, 1044 (1960).

2. I. M. Voskoboinikov, A. V. Dubovick, and V. K. Bobolev, Dokl. Akad. Nauk SSSR 161, 1152 (1965).

3. R. W. Watson, C. R. summers, F. C. Gibson, and R. W. Van Dolah, Proceedings, Fourth Symposium (International) on Detonation ACR-126, Office of Naval Research, Department of the Navy, Washington, D.C., 1966, p. 117.

4. A. B. Amster, D. M. McEachern, Jr., and Z. Pressman, Proceedings, Fourth Symposium (International) on Detonation ACR-126, Office of Naval Research, Department of the Navy, Washington, D. C., 1966, p. 126.

5. R. W. Watson, Twelfth Symposium (International) on Combustion, The Combustion Institute, Pittsburgh, Pennsylvania, 1969, p. 723.

6. R. W. Woolfolk and A. B. Amster, The Twelfth Symposium (International) on Combustion, The Combustion Institute, Pittsburgh, 1969, p. 731.

7. J. Taylor, Detonation in Condensed Explosives, Chapter X, Oxford at the Clarendon Press, 1952.

8. D. C. Wooten, M. Cowperthwaite, and D. C. Erlich, Final Report on SRI Project SCU-7771, "Investigation of Low-Velocity Detonation Phenomena in Liquid Propellants, Fuels, and Explosives," prepared for Director of Aeromechanics and Energetics, Air Force Office of Scientific Research under Contract F44620-69-C-0079, 1972.

9. Ya B. Zeldovich and A. S. Kompaneets, Theory of Detonation, Academic Press, New York and London, 1960.

10. M. Cowperthwaite, Final Report on SRI Project PYU-5918, BRL CR49, "Theoretical Studies of Detonation," prepared for Ballistic Research Laboratories under Contract No. DA-04-200-AMC-2469(X), 1971.

11. R. Courant and K. O. Friedrichs, Supersonic Flow and Shock Waves, Interscience, New York, 1948.

12. M. W. Evans, B. O. Reese, L. B. Seely, and E. L. Lee, Proceedings, Fourth Symposium (International) on Detonation ACR-126, Office of Naval Research, Department of the Navy, Washington, D.C., 1966, p. 359.

13. M. J. Ginsberg, "Effects of Stress on the Electrical Resistance of Ytterbium and Calibration of Ytterbium Stress Transducers," Final Draft Report, Contract DNA001-72-C-0146, Stanford Research Institute, Menlo Park, California (1973).

Appendix

CALCULATION OF THE COLLAPSE OF A VAPOR BUBBLE LEADING TO HOT-SPOT INITIATION

Jay Levine and D. C. Wooten

Ultrasystems, Inc.

Appendix

CALCULATION OF THE COLLAPSE OF A VAPOR BUBBLE LEADING TO HOT-SPOT INITIATION

Introduction

The important role of bubble hot-spot ignition in the initiation and propagation of low velocity detonation (LVD) was discussed in a previous report, and equations were derived that govern the collapse of a spherical vapor bubble.[1] Of interest here is the collapse of a bubble leading to high interior temperatures causing local initiation of reaction which may ultimately ignite the bulk material leading to explosion.

Theoretical studies of hot-spot initiation that are related to the adiabatic compression of a bubble have been carried out by Zinn[2], Enig[3], and Gill.[4] These are computations of ignition delay time which are applicable to a bubble with a stationary radius and with no mass transfer at the bubble wall. In the present computations, however, we are interested in the temperature rise and the onset of reaction or ignition in a collapsing vapor bubble. We include here the effects of both heat and mass transfer (vaporization) at the bubble wall, and formulate the problem in Lagrangian coordinates that move with the bubble wall during collapse. It is assumed that both the vapor and liquid are nonviscous and, prior to collapse, they have the same temperature T_o. The interior of the vapor bubble is assumed to be uniform, an assumption that is justified provided that the thermal diffusivity of the vapor is much greater than that of the liquid and that the speed of the bubble wall motion is much less than the sound speed in the vapor. The first condition is certainly true for most substances for, although the thermal conductivity of the liquid is about ten times greater than that of the vapor, the thermal diffusivity of the vapor is still much greater than that of the liquid. The second condition has been discussed by Hickling[5] in connection with the collapse of a bubble of inert gas in a liquid. Hickling found that the sound speed in the gas was indeed much higher than the velocity of the bubble wall for initial bubble radii of $R_o = 10^{-1}$ to 10^{-3} cm. and overpressures of about 4 atm. Under such conditions, the pressure in the vapor bubble remains approximately uniform because the effects of disturbances at the wall will have time to be propagated throughout the bubble interior. It is clear that during the early stages of collapse the assumption of uniform bubble interior

will certainly be valid in the present calculation. Further, to keep the problem tractable, a spherical bubble will be assumed even though shock compression in general produces asymmetric collapse and, in addition, it s known that spherical bubbles are generally unstable during the latter stages of collapse.

The formulation of the equations to be solved is given in the following section, followed by a discussion of the numerical methods used to solve the equations. The results of several example solutions are then discussed.

Formulation of the Problem

A very general formulation of the equations governing the motion of a bubble in a liquid was given by Hsieh,[6] as well as simplified equations for a spherical bubble with a uniform interior. With the above assumptions and the additional assumptions that:

(1) No body force is present,

(2) There is no translational motion of the bubble relative to the liquid;

(3) Viscosity coefficients are zero throughout;

(4) The liquid is incompressible;

(5) The equation for the temperature in the liquid T_ℓ (r, t) can be written as

$$\frac{\partial T_\ell}{\partial t} + v_\ell \frac{\partial T_\ell}{\partial r} = \alpha_\ell \left(\frac{\partial^2 T_\ell}{\partial r^2} + \frac{2}{r} \frac{\partial T_\ell}{\partial r} \right) \tag{1}$$

where r is the radial coordinate from the bubble center and α_ℓ is the thermal diffusivity of the liquid, which will be assumed constant. Since the liquid is treated as incompressible, and the density of the vapor ρ_v is generally much less than that of the liquid, from the continuity requirement the liquid velocity may be directly related to the bubble radius R(t) as follows:

$$V_\ell = \frac{R^2 \dot{R}}{r^2} \quad . \tag{2}$$

That is, the contribution of mass transfer (vaporization) at the bubble surface to R is neglected. Note that the assumption of uniform bubble interior requires that the quantities inside the bubble ρ_v, T_v, P_v are functions of time only. The initial condition will be that at t=0 a bubble of radius R_o is at rest, with the vapor inside at initial density and pressure of ρ_{vo}, respectively. The assumption of uniform initial temperature T_o for the system requires that

$$T_v(0) = T_\ell(r,0) = T_o \quad . \tag{3}$$

Further, the boundary condition at the bubble wall requires that

$$T_v(t) = T_\ell(0,t) \tag{4}$$

and

$$\lambda_\ell \frac{\partial T_\ell}{\partial r}(0,t) = \frac{L}{4\pi R^2}\frac{d}{dt}\left(\frac{4}{3}\pi R^3 \rho_v\right) + \frac{\rho_v R C_v}{3}\frac{dT_v}{dt} + P_v \dot{R}$$
$$- \rho_v \left(\frac{4}{3}\pi R^3\right) QZ \left(\exp\left[-E/\mathcal{R}T_v\right] - \exp\left[-E/\mathcal{R}T_o\right]\right) \quad (5)$$

when L is the latent heat per unit mass, C_v is the specific heat at constant volume of the vapor, and λ_ℓ is the thermal conductivity of the liquid. The quantities λ_ℓ, L, and C_v are assumed constant, as are Q, Z, and E which denote, respectively, the specific heat of reaction, the frequency factor, and the activation energy. The last term in Eq. (5) is the heat release in the bubble due to gas phase reaction which is generally negligible until T_v reaches the order of $E/\mathcal{R}$.

Since the (uniform) temperature in the vapor bubble is determined by the temperature of the liquid at the bubble wall, it follows that the (uniform) pressure in the bubble P_v is given by the vapor pressure of the liquid at the wall or bubble temperature. We will therefore make the additional assumption that the vapor pressure is the equilibrium vapor pressure at the bubble wall and that the bubble contains pure vapor. Thus, the possibility that absorbed gas in the liquid may contribute to the interior pressure of the bubble is excluded, and the results will be applicable to a pure liquid or to cases in which the partial pressure of absorbed gases is negligible in comparison with the vapor pressure. The equilibrium vapor pressure requirement is certainly valid in the early stages of collapse until the rate of change of the pressure in the bubble becomes comparable to the kinetic rate of vaporization. To enable us to treat the problem analytically, we will relate the vapor pressure of the liquid, and hence the pressure in the bubble, to the temperature at the bubble surface by use of the Calsuis-Clapeyron equation

$$P_v = P_o \exp\left\{\frac{L}{\mathcal{R}T_o}\left(1 - \frac{T_o}{T_v}\right)\right\}, \quad (6)$$

where $\mathcal{R}$ is the ideal gas constant and P_o is the vapor pressure at the initial temperature T_o. Further, the thermodynamic quantities in the vapor phase will be related by the ideal gas equation of state

$$P_v = \mathcal{R}\rho_v T_v \quad . \quad (7)$$

The additional equation required to complete the formulation of the problem is the differential equation for the motion of the bubble wall[26]

$$R\ddot{R} + \frac{3}{2}(\dot{R})^2 = -\frac{(P_\infty - P_v)}{\rho_\ell}, \quad t>0, \tag{8}$$

where P_∞, assumed constant, is the initial pressure in the bulk liquid and corresponds to the pressure at large distance from the bubble during collapse. The initial conditions for Eq. (8) are taken as

$$R(0) = R_o$$

and (9)

$$\dot{R}(0) = 0$$

Equations (1), (2), (6), (7), and (8) now form a set for the dependent variables $V_\ell(r,t)$, $T_\ell(r,t)$, $P_v(t)$, and $\rho_v(t)$, subject to the conditions of (3), (4), (5), and (9).

Introduce the dimensionless variables

$$\begin{aligned} x &= \frac{1}{3R_o^3}(r^3 - R^3(t)) \\ \hat{t} &= t/\tau_c \\ \hat{R} &= R(t)/R_o \\ \theta_v &= \frac{T_v - T_o}{T_o} \\ \theta &= \frac{T_\ell - T_o}{T_o} \end{aligned} \tag{10}$$

and the parameters

$$\begin{aligned} \eta &= L/\Re T_o \\ \tau_c &= (P_\ell R_o^2/P_\infty)^{1/2} \\ \tau_h &= R_o^2/\alpha_\ell \\ \tau_r &= \Re T_o/QZ, \end{aligned} \tag{11}$$

where τ_c is the characteristic time for bubble collapse, τ_h is the characteristic time for heat transfer to the bubble wall, and τ_r is the dimensionless frequency factor for the reaction term in Eq. (5).

Equation (1) can now be written as

$$\frac{\partial\theta}{\partial t} = \left(\frac{\tau_c}{\tau_h}\right) \hat{R}^4 \frac{\partial}{\partial x} \left[\left(1 + \frac{3x}{\hat{R}^3}\right)^{4/3} \frac{\partial\theta}{\partial x}\right] \tag{12}$$

and the conditions (3), (4), and (5) become respectively,

$$\theta_v(0) = \theta(x,0) = 0, \; x \geq 0 \tag{13}$$

$$\theta_v(\hat{t}) = \theta(0,\hat{t}) , \quad \hat{t} \geq 0 \tag{14}$$

and

$$\frac{\partial\theta}{\partial x}(0,\hat{t}) = (\gamma-1)\frac{C_v}{C_\ell}\left(\frac{\rho v_o}{\rho_\ell}\right)\left(\frac{\tau_h}{Z_c}\right)\left(\frac{1}{\hat{R}^2}\right) \exp\left[\eta\left(\frac{\theta_v}{1+\theta_v}\right)\right] \times$$
$$\left\{\frac{d\hat{R}}{d\hat{t}}\left(\frac{\eta}{1+\theta_v}+1\right) + \frac{\hat{R}}{3}\left(\frac{1}{1+\theta_v}\right)\frac{d\theta_v}{d\hat{t}}\left[\left(\frac{\eta}{1+\theta_v}\right)^2 - \frac{\eta}{1+\theta_v} + \frac{1}{\gamma-1}\right] + \right.$$
$$\left.\frac{\hat{R}}{3}\left(\frac{1}{1+\theta_v}\right)\left(\frac{\tau_c}{\tau_r}\right)\left(\exp\left[-\frac{E}{\Re T_o}\left(\frac{1}{1+\theta_v}\right)\right] - \exp\left[-\frac{E}{\Re T_o}\right]\right)\right\} \tag{15}$$

where γ is the ratio at specific heats of the vapor phase and ρ_{vo} is the initial density in the vapor phase.

The bubble equation (8) can be written as

$$\hat{R}\left(\frac{d^2\hat{R}}{d\hat{t}^2}\right) + \frac{3}{2}\left(\frac{d\hat{R}}{d\hat{t}}\right)^2 = -\frac{P_\infty - P_v}{P_\infty} \tag{16}$$

with the initial conditions

$$\hat{R}(0) = 1 \tag{17}$$

and

$$\frac{d\hat{R}}{d\hat{t}}(0) = 0 \; . \tag{18}$$

Equations To Be Numerically Integrated

The nondimensional heat conduction equation (12) in the liquid may be written as

$$\frac{\partial\theta}{\partial\hat{t}} = \frac{\tau_c}{\tau_h}(\hat{R}^3 + 3x)^{1/3}\left[(\hat{R}^3 + 3x)\frac{\partial^2\theta}{\partial x^2} + 4\frac{\partial\theta}{\partial x}\right] \tag{19}$$

Two boundary conditions, an initial condition, and an equation for the bubble radius must be given to complete the specification of the problem. Far away from the bubble surface, the liquid temperature is assumed to be constant, hence,

$$\theta(x \to \infty) = 0 \tag{20}$$

At the bubble surface the energy balance (15) can be written,

$$\left.\frac{\partial\theta}{\partial x}\right|_{x=0} = \frac{P_o R_o}{\lambda T_o}\left(\frac{P_\infty}{\rho_\ell}\right)^{1/2}\frac{1}{\hat{R}^2}\frac{P_1}{P_o}\left\{\left(\frac{\eta}{1+\theta_1}+1\right)\frac{d\hat{R}}{d\hat{t}}\right.$$

$$+\frac{\hat{R}}{3}\left(\frac{1}{1+\theta_1}\right)\frac{d\theta_1}{d\hat{t}}\left[\left(\frac{\eta}{1+\theta_1}\right)^2 - \left(\frac{\eta}{1+\theta_1}\right) + \frac{1}{\gamma-1}\right] \tag{21}$$

$$\left.-\frac{\hat{R}}{3}\left(\frac{1}{1+\theta_1}\right)\left(\frac{QZ\tau_c}{\mathcal{R}T_o}\right)\left(\exp\left[-\frac{E}{\mathcal{R}T_o}\left(\frac{1}{1+\theta_1}\right)\right] - \exp\left[-\frac{E}{\mathcal{R}T_o}\right]\right)\right\}$$

where the pressure ratio P_1/P_o is given by

$$\frac{P_1}{P_o} = \exp\left[\frac{L}{\mathcal{R}T_o}\left(1 - \frac{T_o}{T_1}\right)\right] = \exp\left[\frac{\eta\theta_1}{1+\theta_1}\right] \tag{22}$$

and where the subscript 1 refers to conditions at the bubble wall. The initial condition for equation (19) is

$$\theta(\hat{t} = 0) = 0 \tag{23}$$

The equation for the motion of the bubble wall is

$$\hat{R}\frac{d^2\hat{R}}{d\hat{t}^2} + \frac{3}{2}\left(\frac{d\hat{R}}{d\hat{t}}\right)^2 + \frac{M}{\hat{R}}\frac{d\hat{R}}{d\hat{t}} = -\left(1 - \frac{P_1}{P_\infty}\right) \tag{24}$$

where,

$$\hat{R}(\hat{t}=0)=1 \qquad \frac{d\hat{R}}{d\hat{t}}(\hat{t}=0)=0 \tag{25}$$

Transformed Equations

The temperature gradient is greatest at the bubble surface and decays rapidly with distance into the liquid. For this reason it is desirable to transform to a coordinate system in which constant increments in the transformed plane correspond to very small increments near the surface and ever larger ones as the distance from the surface increases. Also, the boundary condition (20) need not be applied at $x = \infty$, since during the very rapid bubble collapse, the heat transferred from the bubble interior can only propagate a short distance into the liquid. There are many possible coordinate transformations possessing the desired characteristics, the one selected for use in the current analysis is given by,

$$Z=\frac{\Delta Z}{a}\ln\left[1+\frac{x}{\Delta x_o}(e^a-1)\right]$$

or, (26)

$$x=\frac{\Delta x_o}{e^a-1}\left[e^{aZ/\Delta Z}-1\right]$$

This transformation maps the region

$$x=0\rightarrow x_{max}$$

into (27)

$$Z=0\rightarrow 1$$

where,

$$x_{max}=\frac{\Delta x_o}{(e^a-1)}(e^{a/\Delta Z}-1) \tag{28}$$

The step size in the transformed plane, ΔZ, is constant. In the physical plane the first mesh point is a distance Δx_o from the bubble surface. The Δx intervals then grow in an exponential manner as one proceeds away from the surface. The derivatives of the transformation are also required.

Let:
$$\alpha = \frac{\Delta x_o}{(e^a - 1)} \qquad \beta = \frac{a}{\Delta Z} \tag{29}$$

then,

$$\frac{dZ}{dx} \equiv Z' = \frac{e^{-\beta Z}}{\alpha\beta} \tag{30}$$

$$\frac{d^2 Z}{dx^2} \equiv Z'' = -\frac{e^{-2\beta Z}}{\alpha^2\beta} = -Z'^2\beta \tag{31}$$

The following relations can then be used to transform the heat conduction equation (19).

$$\frac{\partial}{\partial x} = Z' \frac{\partial}{\partial Z}$$

$$\frac{\partial^2}{\partial x^2} = Z'' \frac{\partial}{\partial Z} + Z'^2 \frac{\partial^2}{\partial Z^2} \tag{32}$$

The transformed equation becomes,

$$\frac{\partial\theta}{\partial\hat{t}} = \frac{\tau_c}{\tau_n}(\hat{R}^3 + 3x)^{1/3}\left\{\left[(\hat{R}^3 + 3x)\,Z'' + 4Z'\right]\frac{\partial\theta}{\partial Z} + (\hat{R}^3 + 3x)\,Z'^2\frac{\partial^2\theta}{\partial Z^2}\right\} \tag{33}$$

The transformed boundary conditions are:

$$\theta = 0 \text{ at } Z = 1 \tag{34}$$

$$\frac{\partial\theta}{\partial Z}\Big|_{Z=0} = \frac{1}{Z'(0)}\frac{\partial\theta}{\partial x}\Big|_{x=0} \tag{35}$$

The bubble equations (24) and (25) are not affected by the transformation.

Finite Difference Solution

Equation (33) subject to the boundary conditions (34) and (35), and the initial condition (23), is solved using the Crank-Nicolson implicit finite difference scheme. A network of mesh points is created as shown in Figure 1.

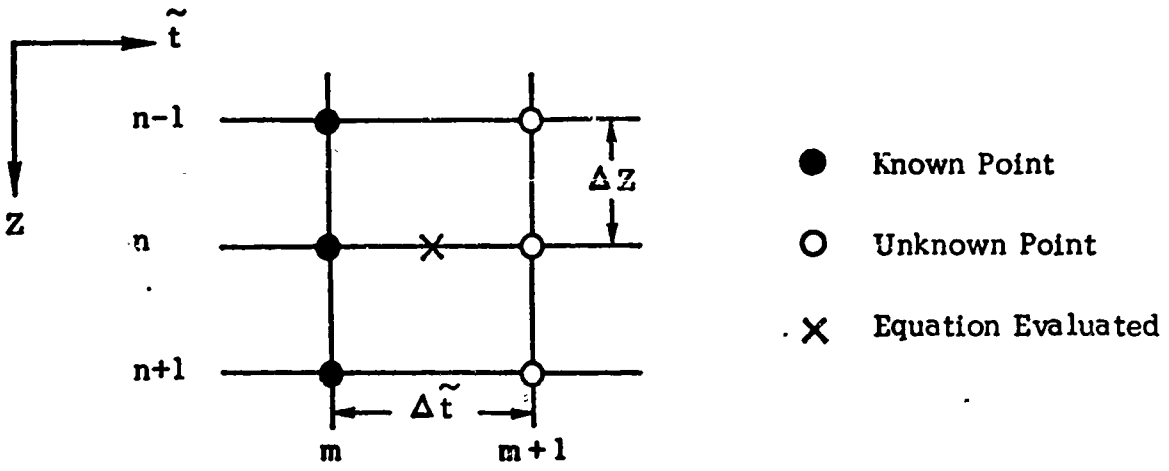

Figure 1. Finite Difference Mesh

With the Crank-Nicholson method the derivatives and coefficients in the differential equation are evaluated at the midpoint m+1/2, n+1/2. The resulting solutions are accurate to second order. For nonlinear problems the difference equations are normally linearized, enabling a solution to be achieved by solving a coupled set of linear, rather than nonlinear, algebraic equations. In such cases, one iteration must be performed to regain second order accuracy. The following representations of the derivatives are used:

$$\frac{\partial\theta}{\partial Z} = 1/2\left[\frac{(\theta_{m,n+1} - \theta_{m,n-1})}{2\Delta Z} + \frac{(\theta_{m+1,n+1} - \theta_{m+1,n-1})}{2\Delta Z}\right] \tag{36}$$

$$\frac{\partial^2\theta}{\partial Z^2} = 1/2\left[\frac{(\theta_{m,n+1} - 2\theta_{m,n} + \theta_{m,n-1})}{\Delta Z^2} + \frac{(\theta_{m+1,n+1} - 2\theta_{m+1,n} + \theta_{m+1,n-1})}{\Delta Z^2}\right] \tag{37}$$

$$\frac{\partial\theta}{\partial\hat{t}} = \frac{\theta_{m+1,n} - \theta_{m,n}}{\Delta\hat{t}} \tag{38}$$

After replacing all of the derivatives in equation (33) by their central difference analogs, (36) to (38), the following set of difference equations is obtained,

$$A_n \theta_{m+1,n-1} + B_n \theta_{m+1,n} + C_n \theta_{m+1,n+1} = D_n \tag{39}$$

$n = 2,3,\ldots N-1$ 1 = surface, N = far boundary

where

$$A_n = (b_n - e_n) \qquad B_n = 1 + 2e_n$$
$$C_n = -(b_n + e_n) \qquad D_n = \theta_{m,n} + b_n \theta_{Z_{m,n}} + e_n \theta_{ZZ_{m,n}} \tag{40}$$

$$\theta_{Z_{m,n}} = \theta_{m,n+1} - \theta_{m,n-1}$$
$$\theta_{ZZ_{m,n}} = \theta_{m,n+1} - 2\theta_{m,n} + \theta_{m,n-1} \tag{41}$$

and,

$$b_n = \Delta t \frac{\tau_c}{\tau_n} \frac{(R^3_{av} + 3x_n)^{1/3}}{4\Delta Z} \left[(R^3_{av} + 3x_n) Z''_n + 4Z'_n \right]$$
$$e_n = \Delta t \frac{\tau_c}{\tau_n} \frac{(R^3_{av} + 3x_n)^{1/3}}{2\Delta Z^2} (R^3_{av} + 3x_n) Z'^2 \tag{42}$$

Once the boundary conditions have been applied, (39) yields a set of N-2, tridiagonal, linear algebraic equations, which may be efficiently solved using a simple Gaussian elimination algorithm. To reduce equations (39) to tridiagonal form the boundary conditions at Z=0 and Z=1 must be used to evaluate the terms

$$A_2 \theta_{m+1,1} \text{ and } C_{N-1} \theta_{m+1,N} \tag{43}$$

The far boundary condition (34) given $\theta_{m+1,N}=0$. The surface boundary condition is nonlinear and may be treated in numerous ways. The method currently being used iteratively selects values for $\theta_{m+1,1}$ until the derivative at the surface given by (35) is equal to the calculated derivative, to within a specified tolerance. The calculated surface derivative is evaluated using a four-point formula

$$\left.\frac{\partial\theta}{\partial Z}\right|_{Z=0} = \frac{(-11\theta_{m+1,1} + 18\theta_{m+1,2} - 9\theta_{m+1,3} + 2\theta_{m+1,4})}{6\Delta Z} \tag{44}$$

The method of solution, as given, assumes that the instantaneous bubble radius is known. In reality, however, the bubble radius is a function of pressure, and, hence, by (22), a function of surface temperature. In order to avoid a simultaneous, iterative, solution of the heat conduction equation and the bubble equation (24), the calculation of the bubble radius is done in an uncoupled manner. This procedure for uncoupling the bubble radius calculation appears to work satisfactorily, and is described below.

The second order bubble differential equation (24) is rewritten as a set of two first order equations,

$$\hat{R}\frac{d\dot{R}}{d\hat{t}} + \frac{3}{2}\dot{R}^2 + \frac{M}{R}\dot{R} = -\left(1 - \frac{P_1}{P_\infty}\right) \tag{45}$$

$$\frac{d\hat{R}}{d\hat{t}} = \dot{R} \tag{46}$$

a simple Euler integration of (45) and (46) is then carried out.

$$\hat{R}_{\hat{t}+\Delta\hat{t}} = \hat{R}_{\hat{t}} + \dot{R}_{\hat{t}}\,\Delta\hat{t} \tag{47}$$

$$\dot{R}_{\hat{t}+\Delta\hat{t}} = \dot{R}_{\hat{t}} - \frac{\Delta\hat{t}}{\hat{R}_{\hat{t}}}\left[1 - \frac{P_1}{P_\infty} + \frac{3}{2}\dot{R}^2 + \frac{M}{\hat{R}}\dot{R}\right]_{\hat{t}} \tag{48}$$

When calculated in this manner, the bubble radius and velocity at $\hat{t}+\Delta\hat{t}$ depend only on previously known values at time = $\hat{t}$. The bubble parameters given by (47) and (48) are then used in evaluating the term R_{av} in (42), and the surface heat transfer rate (21).

Table 1. Input Values for Calculations

R_o	=	.1, .03 cm
T_o	=	300°K
ρ_ℓ	=	1.13 gm/cm^3
P_∞	=	10^7, 10^9 dynes/cm^2
c_ℓ	=	.45 cal/gm°K = 1.9×10^7 erg/gm°K
h_ℓ	=	135 cal/gm = 5.65×10^9 erg/gm
M	=	61 g/g-mole
μ	=	.0062 gm/cm sec (poise)
λ	=	2.15×10^4 erg/cm sec°K
E	=	2.25×10^{12} erg/mole, or 1.125×10^{12} erg/mole
	=	3.69×10^{11} erg/gm, or 1.845×10^{11} erg/gm
Z	=	3.98×10^{14} sec^{-1}
Q	=	4.6×10^{10} erg/gm, or 0.0
γ	=	1.2
$\mathcal{R}$	=	8.317×10^7 ergs/g-mole°C

Example Calculations and Results

The equations for the collapsing spherical vapor bubble were numerically integrated for two values of initial bubble radius and two overpressures, using the values of the parameter shown in Table 1. Test cases were integrated for an adiabatically collapsing bubble and were compared to other investigator's results to provide an initial check of the integration technique. To serve as a basis for comparison, in each case the collapse of a vapor bubble was computed with no heat release in the vapor phase and shown as the Q=0 curve in Figures 1 through 4. The curves of pressure and temperature histories in the bubbles during collapse are plotted as functions of the bubble radius which varies in time very nearly like the radius of a collapsing adiabatic bubble. As shown in Figures 1 and 2, the temperature (and pressure) in the bubble during collapse follow the non-reacting case until a critical temperature is reached where a rapid increase in temperature(pressure)or ignition takes place. Figure 3 shows the effect of different overpressures; the rate of temperature increase at the higher overpressure is greater because less heat is lost to the liquid during the more rapid collapse. Ignition at both values of overpressure, as would be expected, occurs at about the same temperature. The effects of changing initial bubble radius is shown in Figure 4. The larger bubble ignites at an earlier stage of collapse, probably because there is a lower rate of heat transfer per unit mass of vapor in the larger bubble due to the smaller surface to volume ratio of the larger bubble. Thus, in general, larger bubbles and higher overpressure lead to earlier ignition (in terms of bubble radius).

Once bubble ignition occurs, the integration of the governing equations is terminated because the properties change too rapidly for the program to handle. In interpreting these results, it should be realized that several of the assumptions made in deriving the governing equations are not valid during the latter stages of the bubble collapse. For example, as the bubble wall reaches a very high velocity, the assumptions of an incompressible liquid phase and uniform bubble interior are not valid. Also, the assumptions of equilibrium vaporization and reaction kinetics are no longer appropriate for high rates of change of the bubble properties. These results should, therefore, be viewed as a qualitative indication of the effects noted above.

The high pressures generated by the ignition process may cause a reversal of the bubble collapse and a re-expansion of the bubble. The question then arises as to whether the bubble expansion would extinguish the reaction or whether the reaction would continue to drive the bubble past its original size. If the latter occured, this could be taken as a criterion for the ignition of a bulk-cavitated liquid containing many bubbles.

The solution of the rebounding bubble, which requires that liquid compressibility and finite rate kinetics be included in the model may, therefore, lead to an ignition criterion for LVD and other hot-spot ignition phenomena.

REFERENCES

1. Wooten, D. C., Cowperthwaite, M. and Erlich, D. C., "Investigation of Low-Velocity Detonation Phenomena in Liquid Propellants, Fuels, and Explosives", Final Report, AFOSR Contract F44 620-69-C-0079, SRI Project SCR-7771, June 30, 1972.

2. J. Zinn, "Initiation of Explosions by Hot Spots", J. Chem. Phys., 36, 1949 (1962).

3. J. W. Enig, "Approximate Solutions in the Theory of Thermal Explosions for Semi-Infinite Explosives", Proc. Roy. Soc. A. 305, 205 (1968).

4. S. P. Gill, "Initiation and Decomposition of Nitromethane at 10-kbar Pressure", Physics International Technical Report-70-2, March 1970.

5. R. Hickling, "Effects of Thermal Conduction in Sonoluminescence", J. Acoust. Soc. Am., 35, 967 (1963).

6. D. Y. Hsieh, "Some Analytical Aspects of Bubble Dynamics", J. Basic Eng., 87, 991 (1965).

7. H. S. Carslaw, and J. C. Jaeger, Conduction of Heat in Solids, Second Ed., Oxford University Press, London (1959).

Figure Captions

Figure 1. Collapse of vapor bubble with overpressure of 10^7 dynes/cm^2 and intial radius of 0.1 and showing effects of different activation energies compared to bubble collapse with no heat release or reaction (Q=0).

(a) Temperature at the bubble wall vs. bubble radius
(b) Pressure in the bubble vs. bubble radius

Figure 2. Same calculation as in Figure 1 but with a higher overpressure, 10^9 dynes/cm^2.

(a) Temperature at the bubble wall vs. bubble radius
(b) Pressure in the bubble vs. bubble radius.

Figure 3. (a) Bubble wall temperature and
(b) pressure in the bubble during collapse compared for the two different overpressures.

Figure 4. (a) Bubble wall temperature and
(b) pressure in the bubble during collapse compared for two different initial radii.

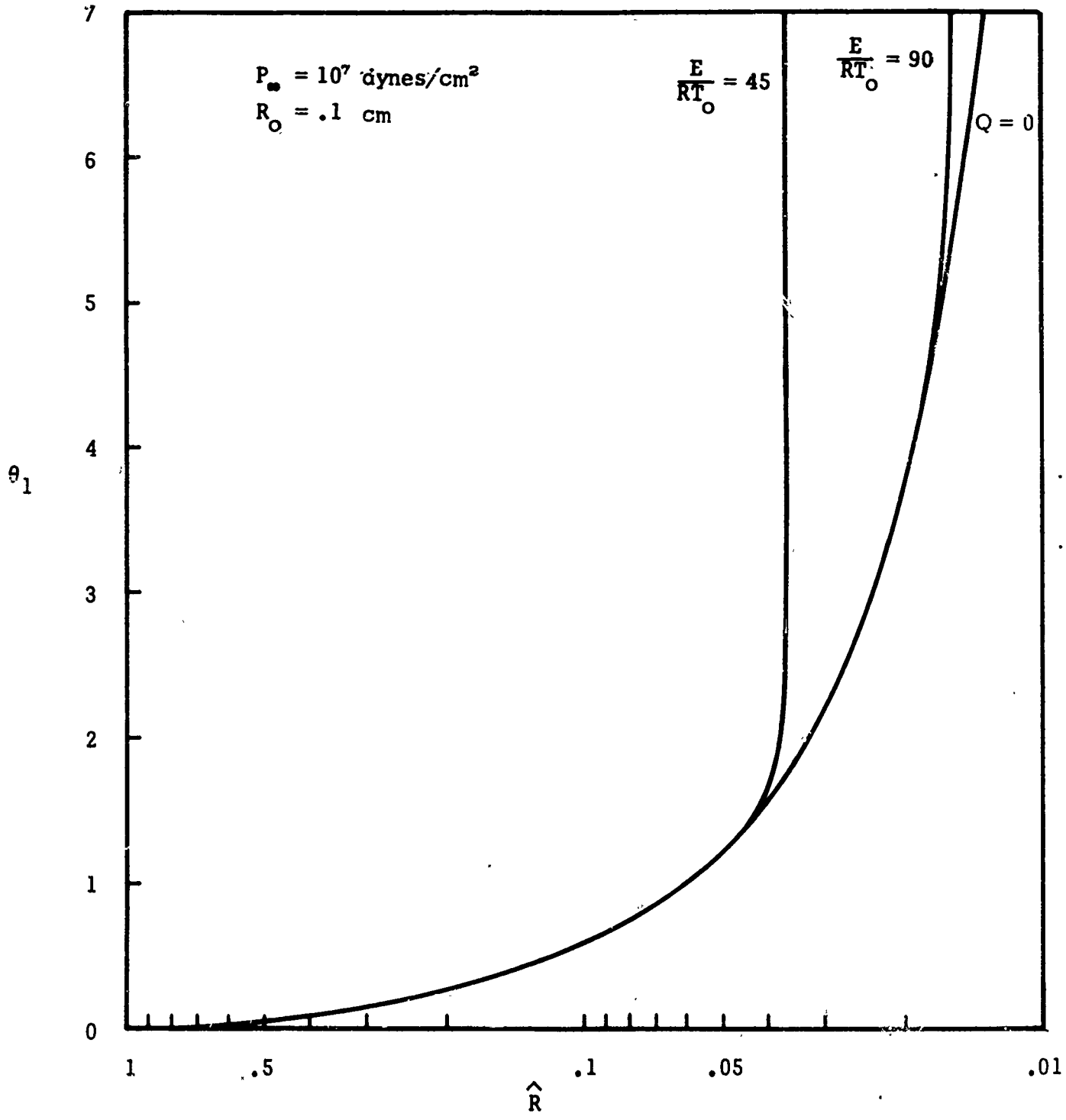

Figure 1a. Temperature At The Bubble Wall vs. Bubble Radius.

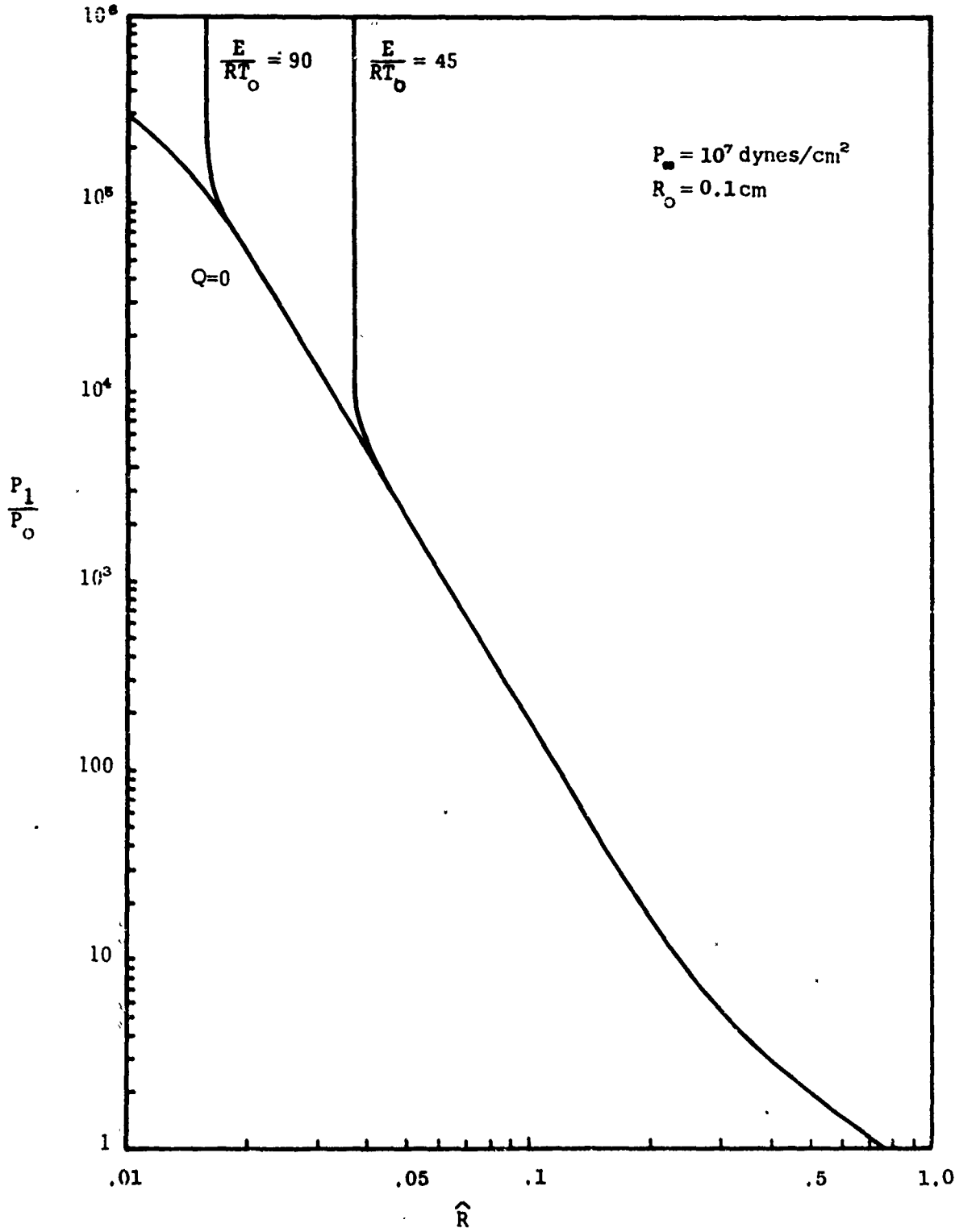

Figure 1b. Pressure In The Bubble vs. Bubble Radius.

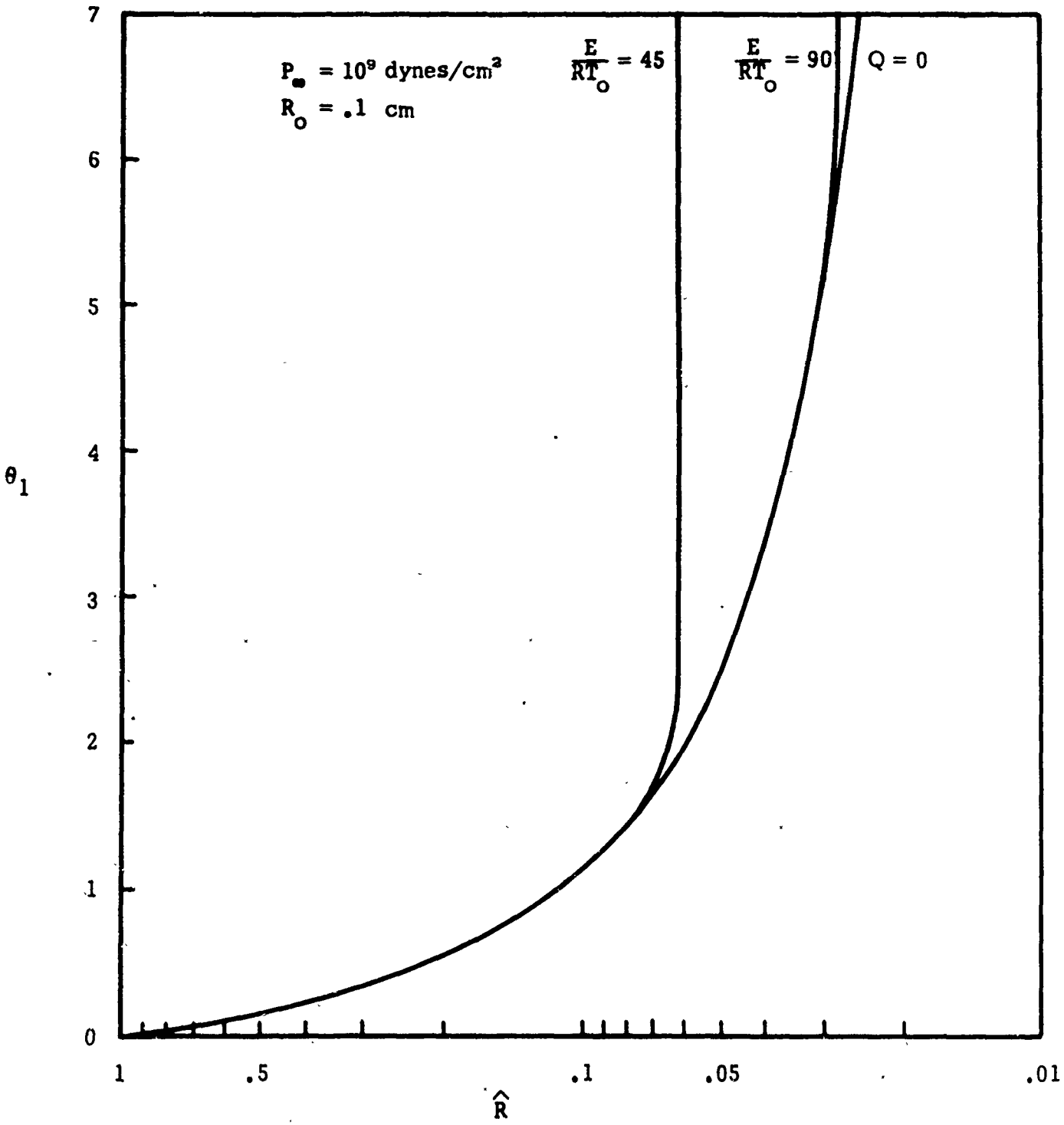

Figure 2a. Temperature At The Bubble Wall vs. Bubble Radius.

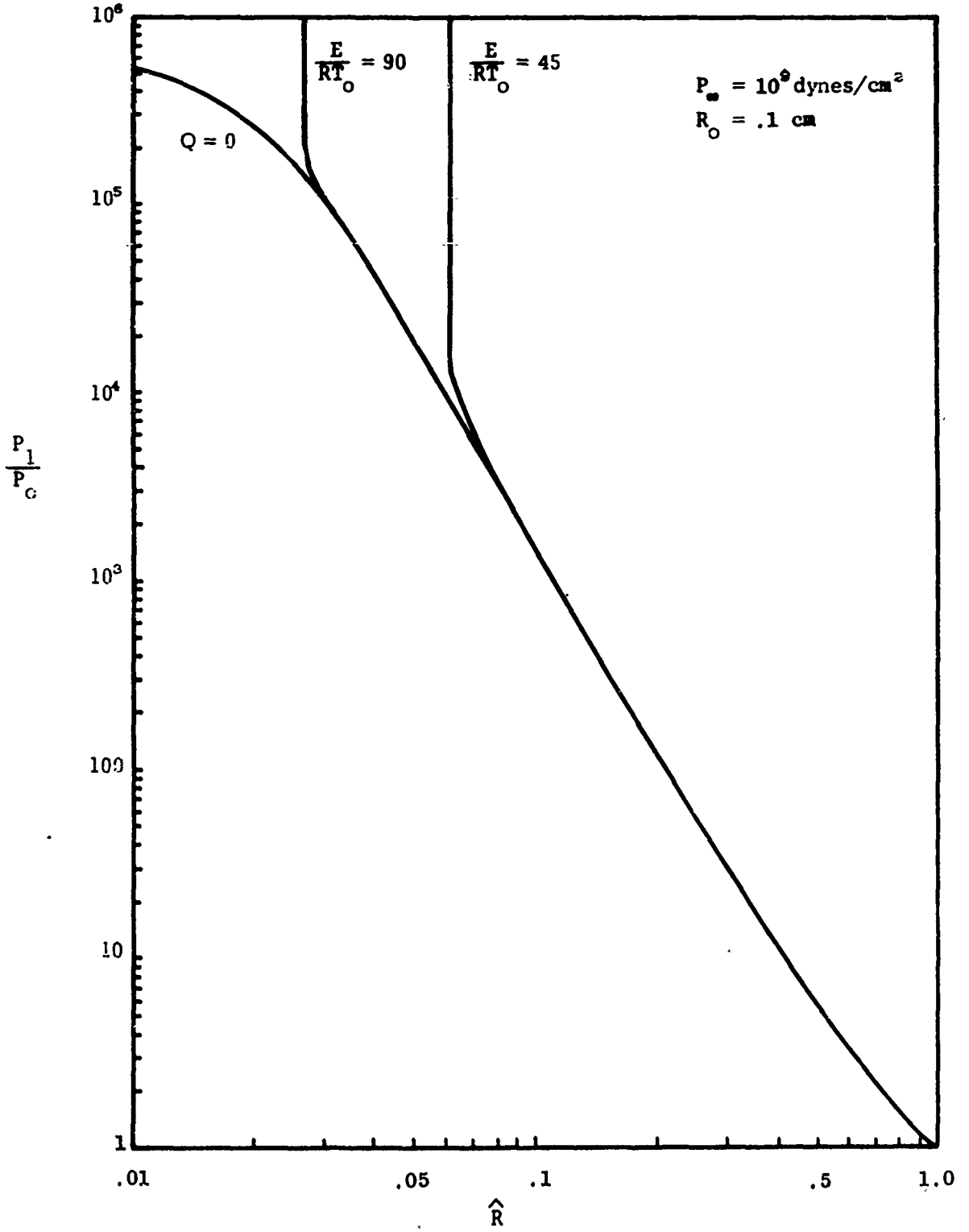

Figure 2b. Pressure In The Bubble vs. Bubble Radius.

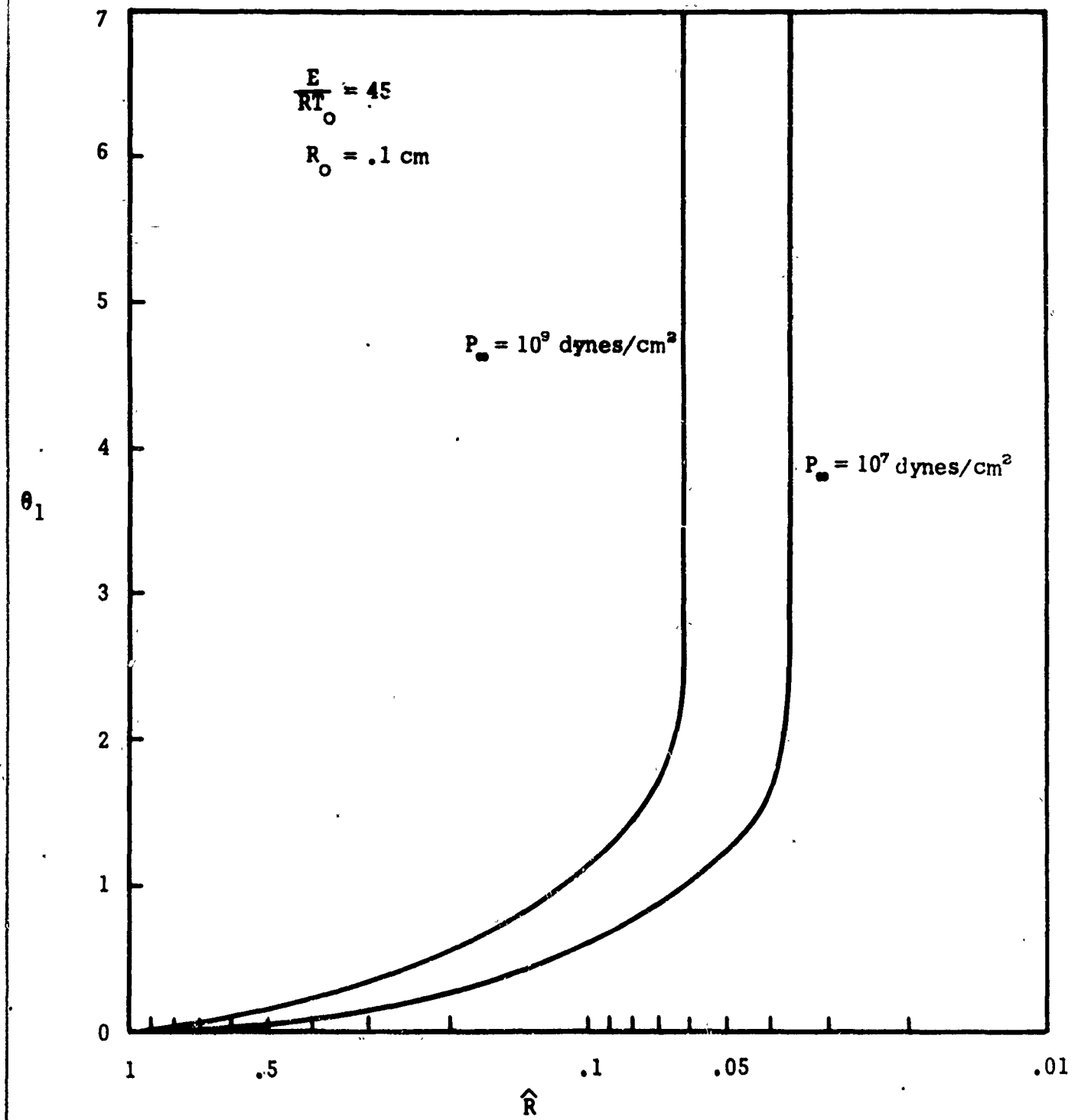

Figure 3a. Bubble Wall Temperature

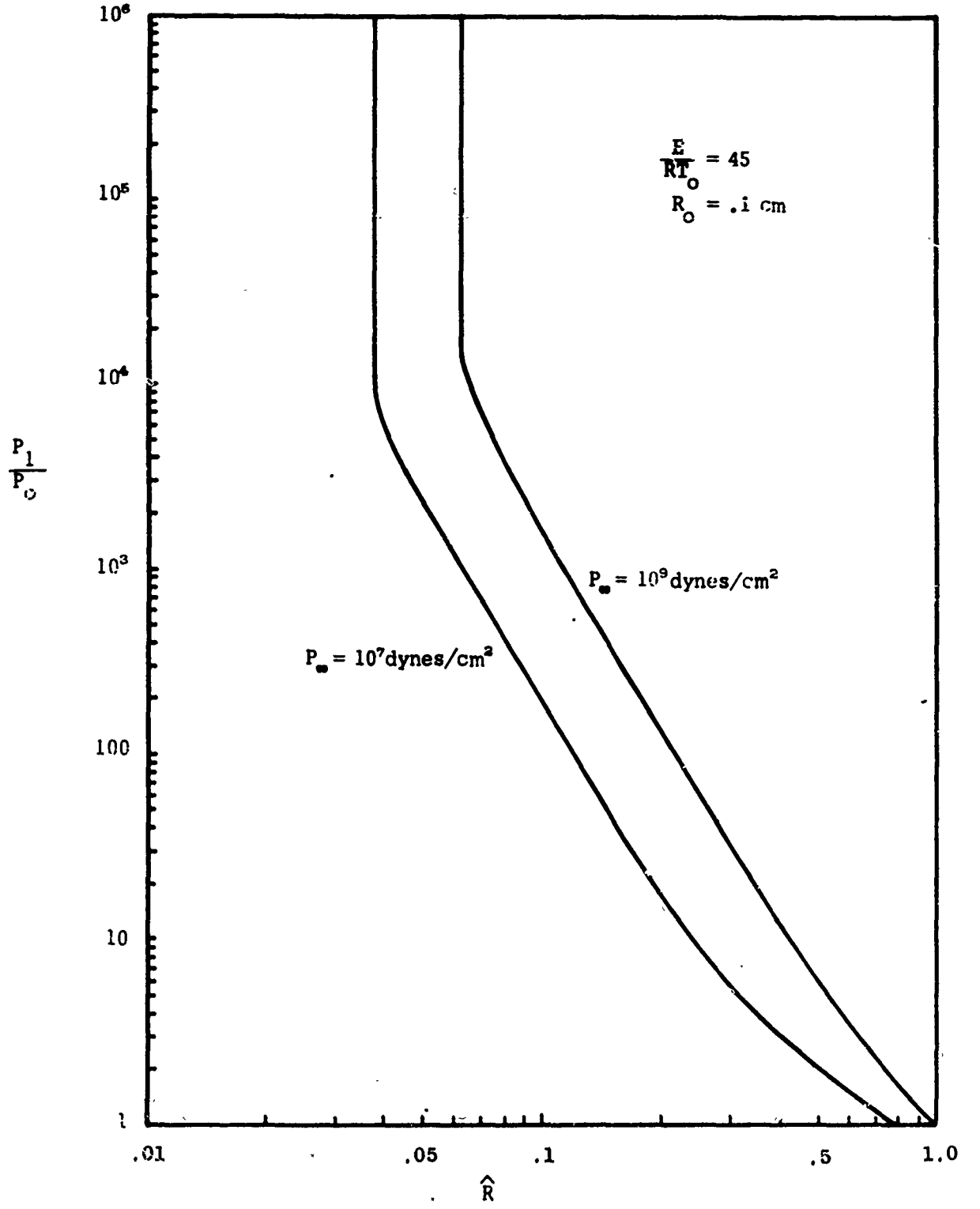

Figure 3b. Pressure In The Bubble During Collaspe Compared For The Two Different Overpressures.

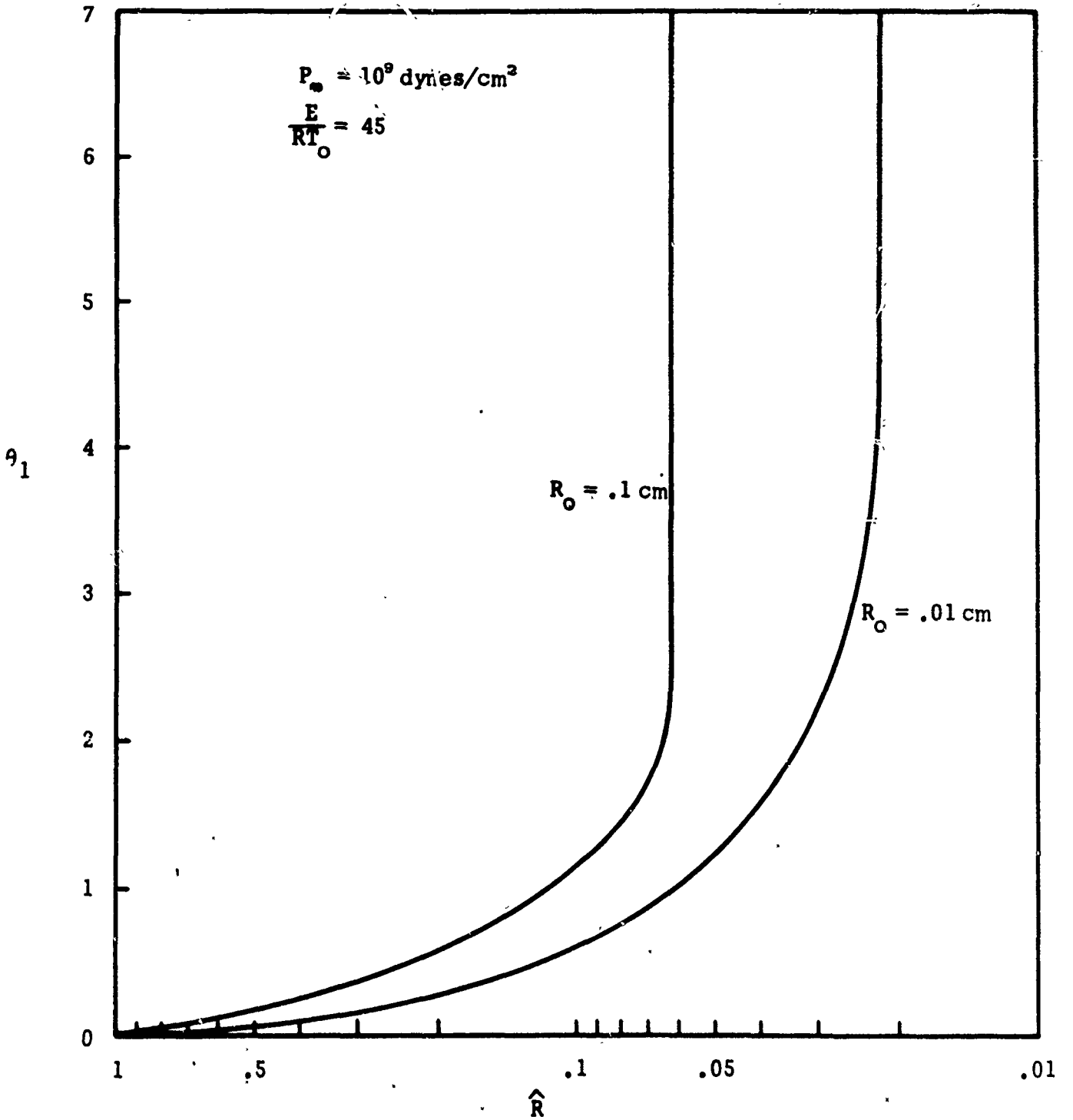

Figure 4a. Bubble Wall Temperature

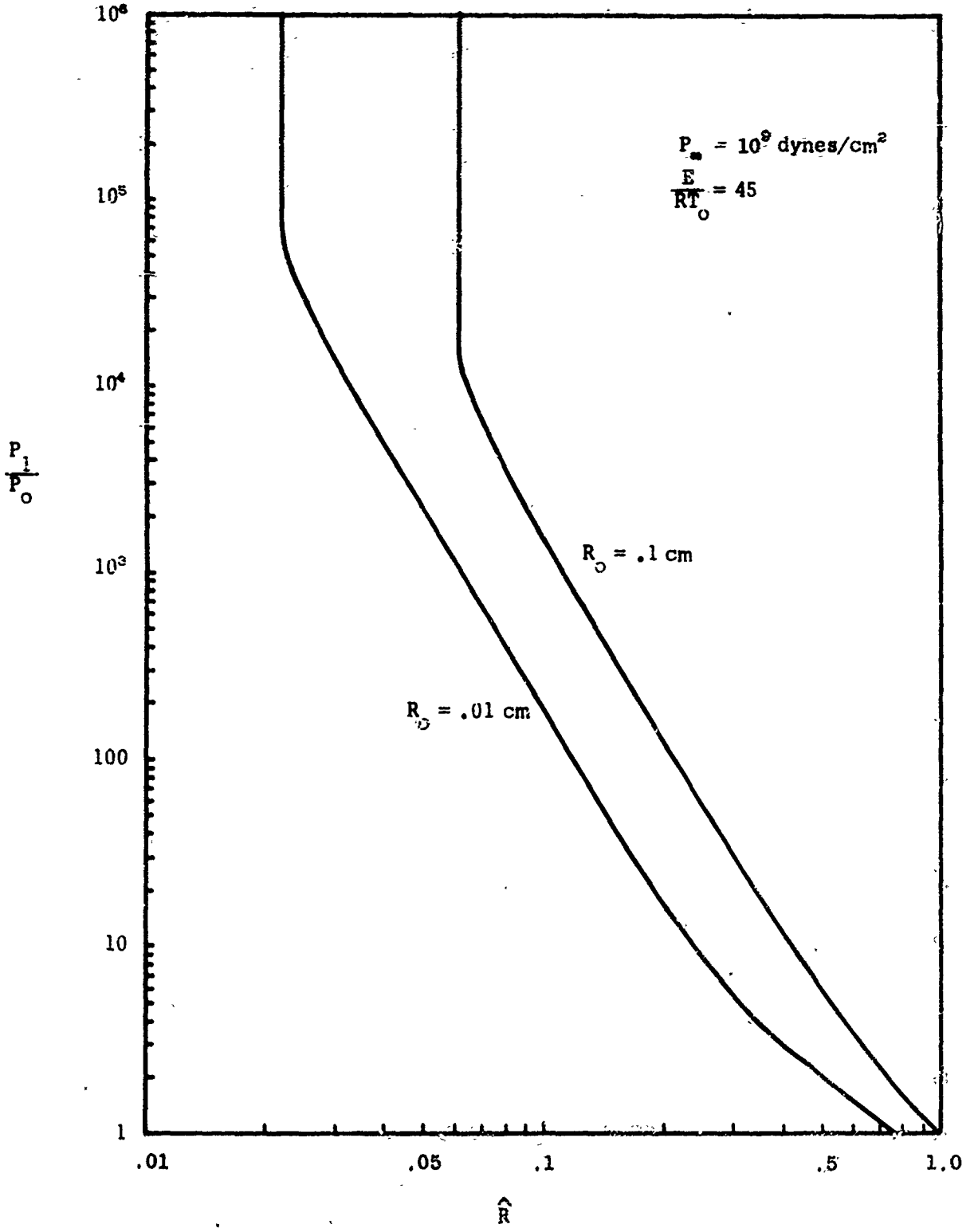

Figure 4b. Pressure In The Bubble During Collapse Compared For Two Different Initial Bubble Radii.